Energy Conversion and Management: X 30 (2026) 101765

Contents lists available at ScienceDirect

Energy Conversion and Management: X

journal homepage: www.sciencedirect.com/journal/energy-conversion-and-management-x

Techno-economic and uncertainty-aware optimization of hybrid renewable systems with small-scale prime movers for commercial buildings

Aggelos Gaitanis [a,*], Diederik Coppitters [b], Ward De Paepe [a,c], Francesco Contino [b]

[a] UMONS Micro gAsturbine Research Centre - UMARC, Thermal Engineering and Combustion Unit, University of Mons (UMONS), rue de l'Epargne 56, Mons, 7000, Hainaut, Belgium

[b] Institute of Mechanics, Materials and Civil Engineering (iMMC), Université catholique de Louvain (UCLouvain), Place du Levant, 2, Louvain-la-Neuve, 1348, Walloon Brabant, Belgium

[c] WEL Research Institute, avenue Pasteur, 6, Wavre, 1300, Belgium

ARTICLE INFO

Keywords:
Techno-economic
Optimization
Uncertainties
Renewables
mGT
ICE
Humidification

ABSTRACT

The increasing share of renewables forces combustion-driven power generation machines to operate with high adaptability. Small-scale heat and power units, like micro gas turbines (mGT), could show potential for Hybrid Renewable Energy Systems (HRES) due to their operational and fuel flexibility. However, their economic viability in a variable energy environment remains uncertain. The levelized cost of exergy (LCOX) in HRES with combined heat and power (CHP) units, should be calculated under uncertainties to support decision-making. This paper applies design optimization to a photovoltaic/battery/heat pump system with two prime movers to investigate the required economic relevance of small-scale CHP units in HRES. The considered prime movers are internal combustion engines (ICE) and mGTs, including advanced mGT configurations such as humidified cycles (mGT-wet, mHAT). Test cases include a hospital, office and hotel in Brussels with distinct demand profiles. Uncertainty quantification on optimized system capacities is performed using Polynomial Chaos Expansions (PCE), ensuring computational efficiency. The hospital shows that adding an mGT improves LCOX (227 €/MWh compared to 244 €/MWh of non-PM HRES), while in the hotel case, non-PM systems are more cost-effective due to low electricity demand. Dry mGTs and ICEs enhance flexibility in HRES for suitable applications, but their economic viability depends strongly on energy prices and demand. Humidified mGTs improve self-sufficiency but with higher fuel cost, making their cost-effectiveness questionable if excess electricity is not sold to the grid.

1. Introduction

The global energy landscape is transitioning towards decentralization with increasing reliance on renewable energy sources. Recent global data show a continued rise in photovoltaic deployment. Solar PV supplied about 5.4% of global electricity generation in 2023, following an annual increase of roughly 320 TWh [1]. Projections from the International Energy Agency indicate that PV will become the largest renewable electricity source by 2029 [1]. The IEA PVPS programme reports that global installed PV capacity passed 1.6 TW in early 2024 [2]. This underlines the accelerated global adoption of solar energy, reflecting the reality of the next decades. Additionally, the Net Zero Emissions by 2050 Scenario foresees further growth of solar PV and wind together with higher electricity demand driven by electrification. To accommodate the integration of accelerated adoption of PV in the energy mix, thermal and grid-scale storage will play a key role to ensure system stability [3].

Many contributions examine microgrids in commercial applications to evaluate their economics, renewable integration, storage and policy conditions. Uddin et al. [4] highlighted the potential importance of microgrids, presenting economic and regulatory challenges. Boruah et al. [5] conducted a comprehensive design and economic feasibility analysis of a commercial grid-connected PV plant with a bank of batteries introducing a novel net-zero energy management system for an educational institution and enhancing grid stability in peak load management. Isa et al. [6] study on a grid-connected hybrid cogeneration system of PV, fuel cells and batteries hospital building offered a practical alternative to traditional power systems. Related work also shows how the integration of heat pumps and thermal

* Corresponding author.
E-mail address: angelosevripidis.gaitanis@umons.ac.be (A. Gaitanis).

https://doi.org/10.1016/j.ecmx.2026.101765
Received 8 December 2025; Received in revised form 16 February 2026; Accepted 12 March 2026
Available online 18 March 2026

storage with battery systems increases on-site PV utilization [7]. Further evidence of economic feasibility is provided by Taghavifar and Zomorodian [8], who reported positive financial outcomes for an on-grid PV–wind hybrid system at a university campus through controlled export of surplus electricity.

In parallel, for remote and residential applications, hybrid renewable microgrids have been shown to present economic potential. Ji [9] reported an islanded PV, wind and biogas microgrid supplying over 90% renewable electricity at a levelized cost of about $0.116/kWh. Similarly, Masrur et al. [10] presented that replacing diesel power generation with solar–wind–battery system decreased both energy costs and carbon emissions. Furthermore, Amini et al. [11] showed that policy incentives further improve economic performance and renewable penetration.

Several articles have been published using optimization on hybrid renewable energy systems. Thus, Güven et al. applied advanced metaheuristic optimization showed significant reductions in total system cost and high renewable penetration under multi-objective schemes [12]. Other studies compared multiple metaheuristic algorithms across grid-connected hybrid designs showing that algorithm selection influences possible renewable shares and levelized costs of energy [13]. Hybrid energy storage concepts combining batteries and supercapacitors have been optimized highlighting the role of focused sizing and dispatch in improving system reliability and cost [14]. Kushwaha and Bhattacharjee effectively optimized of an off-grid microgrid design for rural power supply using slime mould algorithm and reported cost and reliability outcomes for PV–wind–battery–diesel and methanol generators under multiple objective criteria [15]. Hybrid microgrids combining renewable generation, storage have also been optimized using quadratic interpolation based bio inspired algorithms, with applications to commercial buildings and electric vehicle charging infrastructure [16].

As energy systems integrate more renewables, the function of thermal units shifts, yet they still provide needed flexibility and system support [17]. Storage, biomass units, and thermal plants equipped for clean fuels or carbon capture are expected to supply part of this flexibility. In parallel, combined heat and power production from gas turbines, steam turbines [18] and internal combustion engines [19] remains relevant in settings where heat demand is stable. Hospitals fall into this category because hot water and heating loads are high throughout the year, and several medical processes require continuous thermal supply [20].

Micro gas turbines (mGTs) offer a compact and modular option for distributed power generation in microgrids [21]. Interest in these units has increased over the past two decades. Their size, power range of 20–500 kW, fuel flexibility and relatively low emissions make them suitable for dispatchable operation. Previous work has examined the use of mGTs in a wide set of applications. Kumar et al. [22] assessed a hybrid renewable energy system (HRES) featuring PV, batteries, mGT, a desalination unit, and a gasifier for electricity, water, and cooking gas supply in remote Indian locations. The system showed 80 423 kWh/year electricity and 34 778 MJ/year heat output and could produce 9516 l/day freshwater using waste heat from the mGT. Ismail et al. [23] looked at a hybrid system with PV panels, batteries, and a mGT to power remote communities in Palestine. They showed that it was technically and economically possible with a mix of PV panels, battery units, and a 30 kW mGT capacity. Comodi et al. [24] investigated a grid-connected 100 kW mGT combined with a PV array to firm intermittent solar output. Their analysis showed that a hybrid mGT–PV layout can reduce natural gas use by about 16% and lower the specific energy cost compared with a standalone mGT, while also improving supply reliability. A recent review by Weerakoon and Assadi [25] reports similar findings and stresses that coupling mGTs with renewable sources improves both cost performance and efficiency. Other work examines a smart-grid and island configuration in which an Aurelia A400 operates in combined heat and power (CHP) mode together with renewables and storage, depicting the benefit of advanced EMS strategies in such systems [26].

Economic assessments of advanced mGT cycles have also been carried out. Montero Carrero et al. [27] compared an mHAT cycle with a conventional mGT and an ICE unit in CHP for residential buildings. The mHAT presented the highest economic return due to its improved heat flexibility and higher electrical efficiency. A later study [28] indicated that, under current European conditions, mHAT systems remain financially unattractive without stronger incentives. Solar-assisted mGT concepts have also been explored. Coppitters et al. [29] demonstrated that adding concentrating solar power to an mGT cogeneration system for remote supply and desalination increases electrical efficiency by roughly 3.2% points. The proposed design could produce potable water at a cost (≈$1.8–1.9 per m^3/day) comparable to conventional solar-driven desalination plants, showing the techno-economic feasibility of mGTs for combined energy and water production in off-grid applications.

In the above-mentioned design and feasibility assessments for hybrid renewable energy systems, various techno-economic factors are crucial in determining the system's performance. These factors are typically considered fixed or deterministic, matching nominal conditions or scenarios. However, uncertainties like changes in market conditions, adjustments in how people use energy in a building, and yearly variations in solar irradiance can lead to fragile, suboptimal solutions that perform well under idealized assumptions but collapse when reality deviates from predictions [30,31]. Therefore, including uncertain parameters in the design and evaluation process is important, allowing for a more realistic and adaptable approach in decision-making [32]. Furthermore, a comparative uncertainty-based techno-economic evaluation of small-scale prime movers, particularly mGT technologies within commercial HRES applications, remains largely unexplored.

This study contributes to the literature in three ways. First, it provides a direct techno-economic comparison between ICE and mGT technologies within a unified photovoltaic–battery–heat pump framework to assess a possible economic potential in such renewable systems. We chose to contrast mGT with ICE because ICEs typically dominate the small-scale CHP market due to their lower capital expenses (CAPEX). This study also evaluates the impact of water injection on the mGT's cost-effectiveness in delivering heat and electricity including two humidified mGT cycles (mGT-wet and mHAT). Second, it integrates uncertainty quantification of optimized system capacities using Polynomial Chaos Expansions, enabling assessment of performance variability under realistic uncertain economic and climatic inputs. Third, the framework is applied to three distinct commercial building profiles (a hospital, an office and a hotel) in Brussels, Belgium to evaluate how demand structure influences the economic suitability of different prime mover technologies. The optimization simultaneously minimizes the levelized cost of exergy (LCOX) and maximizes self-sufficiency (SSR), allowing consistent comparison across technologies under identical assumptions. Therefore, the novelty of the present study lies in their integrated application within a unified multi-objective and uncertainty-aware optimization framework focusing on small-scale CHP units in HRES.

2. Methodology

The climate data used in the analysis are presented first, showing the values of ambient temperature and solar irradiance throughout the year. These values are used as input parameters in the HRES model. The different demand profiles for this analysis are depicted next, explaining how they are acquired. The energy management system (EMS), along with the methodology behind the modeling of the different components of the system, is thoroughly described. Emphasis is given to calculating prime movers curves of electrical efficiency and thermal power output. The design parameters and objectives are presented and the uncertainties, the polynomial chaos expansion (PCE) and multi-objective optimization algorithm of the system are also depicted.

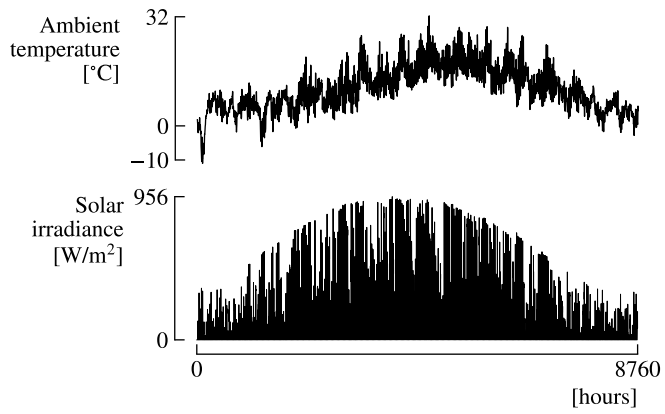

Fig. 1. The hourly ambient temperature and solar irradiance profiles for the city of Brussels are taken from the National Renewable Energy Laboratory [33].

2.1. Climate and demand data

Solar irradiance, the surrounding temperature, and the building's needs for electricity and heating all impact how much energy a grid-connected commercial building uses. For accurate analysis, these climatic conditions are tailored to the location in Brussels city. Given that a building's energy demands are weather-dependent, aligning climate data with energy demand profiles is essential. For the climate conditions, Typical Meteorological Year data was utilized that is provided by the National Renewable Energy Laboratory [33]. Fig. 1 shows the ambient temperature and solar irradiance throughout the year for the city of Brussels.

Codeminders [34] database is applied to compare the meteorological data from Brussels to a specific location in the United States of America (USA). Therefore, a climatic American equivalent for the city of Brussels is located in the city of Portland. For this specific US city, the hourly energy demand data is provided by Open Energy Information [35]. As this database contains hourly heat and electricity data based in cities across the US. This data aids in constructing a realistic representation of the energy demands. The demand profiles for a hospital, an office and a hotel in Portland are acquired. To further customize demand profiles to the average energy consumption for each commercial building in Belgium, the methodology from Montero Carrero et al. is implemented [28]. The demand profiles for a hospital, an office and a hotel in Portland are acquired with 99% match of Brussels climate. Using the data provided by the Institute for Consultancy and Studies on Sustainable Development's [36], the electricity and heating profiles for each commercial building are sized to take into account the cultural differences of the nations.

Fig. 2 shows the sized demand profiles corresponding to three different commercial buildings. The hospital building presents high heating demand as its facilities are used all year. Also, various medical equipment require a steady supply of steam [20]. Thus for the hospital case, the heat demand of the building is divided as heat in the form of steam and heat in the form of hot water. It is assumed that 60% of the total heat demand is satisfied with steam generation and 40% with hot water. This number is in accordance with Chiang et al. [37] as high amount of steam is used for drying (laundry) and sterilization.

The office demand profile presents high electricity requirements and intermittent heat. However, electricity and heat show similar maximum values. The demand profiles of the hotel case presents more distributed heat and electricity requirements than the hospital and office. Also, the maximum heat and electricity demands are significantly lower than the office and hotel. The heat demand in the office and hotel case involves only space heating with hot water. These three profiles have distinct characteristics that can highlight the possible potential of an HRES coupled with a prime mover.

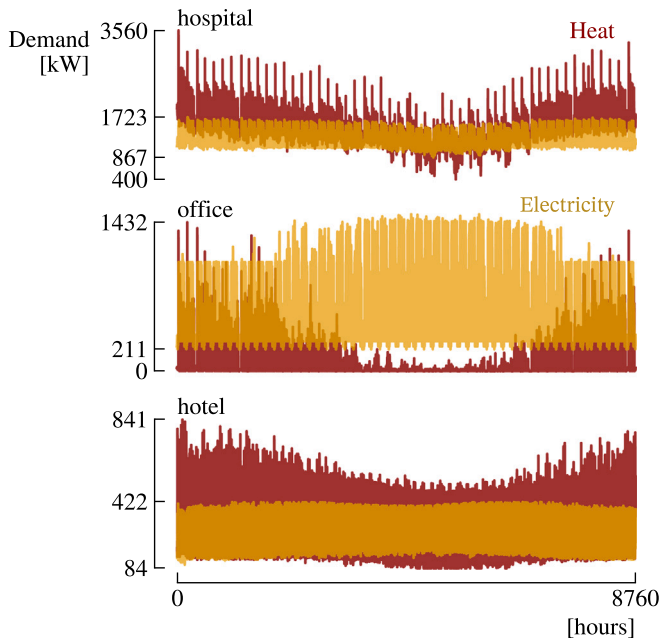

Fig. 2. The hourly heat and electricity profiles for three different commercial buildings located in Brussels. The heat requirements for the three cases drop during the spring and summer period.

Table 1
Seasonal electricity and heat loads demands for the 3 buildings.

Case		Winter	Spring	Summer	Autumn
Hospital [MWh]	Elec. load	2823	2870	2736	2900
	Heat load	3379	2965	2558	3266
Office [MWh]	Elec. load	1161	1431	1742	1310
	Heat load	339	95	23	241
Hotel [MWh]	Elec. load	538	601	623	565
	Heat load	806	647	548	689

To provide a clearer overview of the demand characteristics of the three case studies, Table 1 presents the aggregated calendar seasonal electricity and heat loads. The hospital exhibits high and relatively stable electricity and heat demand throughout the year, while the office shows strong seasonal variation in heat demand and increasing electricity demand in summer. The hotel presents moderate seasonal variation with comparable electricity demand across seasons and higher heat demand in winter.

2.2. Model of the system

The EMS, shown in Fig. 3, handles the flow of energy and is designed to maximize renewable energy use in the system. In this study, the building is connected to the grid. Fig. 3 shows the different technologies of the HRES. This building is equipped with a PV array and a bank of batteries, primarily serving electrical needs, including appliances and lighting. Two technologies are considered for meeting the heating needs. In the first case (PV/battery/heat pump), a heat pump and an electric heater are applied. The electric heat is utilized whenever the heat pump capacity cannot fulfill the demand. In the second case, the PV/battery/heat pump technology is coupled with a prime mover (PM) connected to the gas grid. The prime movers that are compared in this analysis are the ICE, mGT, mGT with liquid water injection (mGT-wet) and mGT with humidification using a saturator (mHAT). Only in the hospital case, an electrical steam generator (ESG) is added to satisfy the high steam demand.

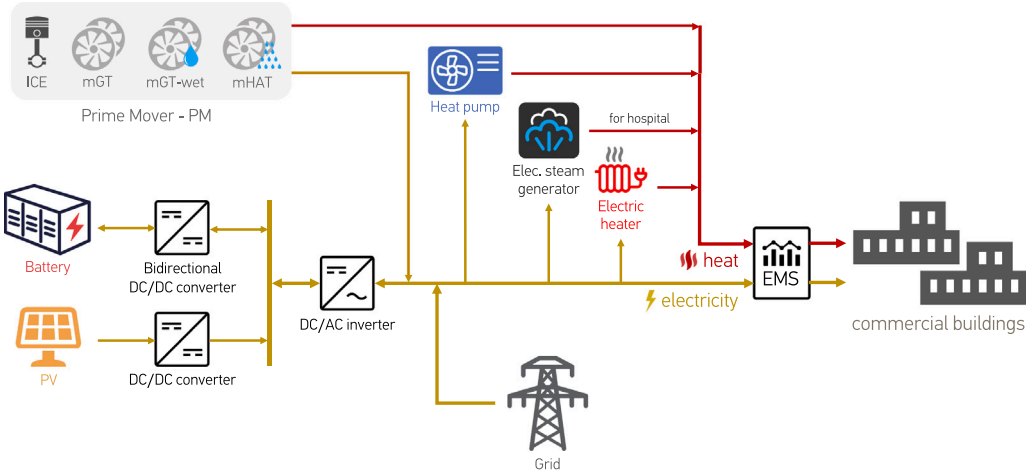

Fig. 3. Layout of the hybrid renewable energy system with a prime mover for backup power. Two systems are considered. A PV/battery/heat pump is compared with a PV/battery/heat pump/prime mover. The two systems are connected to the grid, and an electric heater is also used to cover the demand peaks. The electrical steam generator is only utilized in the hospital case.

In both configurations, the electricity generated by the PV panels is utilized to meet the building's electrical needs. Any excess PV electricity is initially used to operate the heat pump, with any remaining surplus then stored in the battery. Conversely, when the building's electricity demand surpasses the PV output, the system first draws power from the battery to increase the grid independence of the system. Then, the PM is used whenever it is part of the design. The grid electricity is the last resort of the system.

The heat demand fulfillment strategy is complex and involves various decision commands utilizing different technologies. Thus, we first describe the required steps without PM. In the next paragraph, we explain the decision-making logic with the use of PM. When the PM is not considered, the heat demand is covered first by the heat pump. If there is no sufficient excess PV power to run the heat pump to cover the heat demand, the heat pump is operated with the remaining stored energy from the battery. If the electricity demand is not covered by the PV, the battery will first comply with the electricity requirement and if any excess power is left, it will run the heat pump. When the electricity from the battery still cannot run the heat pump to cover the heat demand, the heat pump is operated with the electricity from the grid.

In the case that the prime mover is commissioned (PV/battery/heat pump/prime mover), at first the heat pump runs with electricity either from the excess PV power or the energy in the battery applying the same conditions as in the case of PV/battery/heat pump. When renewable energy is not enough to run the heat pump and cover the remaining heat demand, the PM is applied. The electrical output of the PM is directed to run the heat pump. Therefore, the thermal output of the PM, together with the heat from the heat pump, are added to cover the heat demand as defined by

$$Q_{\mathrm{dem,w}} = \mathrm{COP} \cdot P_{\mathrm{PM,w}} + Q_{\mathrm{PM,w}}, \tag{1}$$

where $Q_{\mathrm{dem,w}}$ is the heat demand in hot water, COP is the coefficient of performance for the heat pump, $P_{\mathrm{PM,w}}$ is the PM electrical output and $Q_{\mathrm{PM,w}}$ is the PM thermal output as a function of the electrical PM power. If there is still demand for heat, the heat pump runs on electricity from the grid.

In the next step, the EMS controls the steam generation based on the steam demand. Only in the hospital case and in the PV/battery/heat pump/prime mover configuration, if the electricity from PV and bank of batteries is not enough to run the steam generator and fulfill the steam demand, the prime move is employed. The prime mover generates steam only in the nominal conditions so the equation to satisfy the steam demand is

$$Q_{\mathrm{dem,s}} = \eta_{\mathrm{ESG}} P_{\mathrm{PM,s}} + Q_{\mathrm{PM,s}}, \tag{2}$$

where $Q_{\mathrm{dem,s}}$ is the heat demand for steam, η_{ESG} is the efficiency of the steam generator (99%) [38], $P_{\mathrm{PM,s}}$ is the electrical output and $Q_{\mathrm{PM,s}}$ is the PM's thermal output in the form of steam. The steam generation of the mGT is discussed in the next section. Therefore, the total produced electricity from the prime mover is $P_{\mathrm{PM}} = P_{\mathrm{PM,w}} + P_{\mathrm{PM,s}}$. Also, both Eq. (1) and (2) apply only when the electricity demand is satisfied from renewables and there is a remainder heat demand. The split fraction of electrical output for PM (P_{PM}) together with the value of P_{PM} are determined with the root-finding python solver, fsolve [39] that minimizes $Q_{\mathrm{dem,w}}, Q_{\mathrm{dem,s}}$. Finally, in case of a demand peak and thus the heat pump capacity cannot satisfy it, an electric heater is used in both cases (PV/battery/heat pump, PV/battery/heat pump/prime mover). This happens when the remaining heat demand is higher than the maximum thermal power that the heat pump can produce.

Fig. 4 shows the power management strategy described in the above-mentioned paragraphs. The system is evaluated every hour of the year. Dynamic transients such as start-up losses, ramp rates, and short-term thermal inertia are not modeled. The calculation starts by comparing the demanded electric power with the electricity produced by the PV. Fig. 4 is divided into five sections (a–e). Area 'a' shows the case when there is excess electricity from PV in a specific hour. This surplus electricity is used to run the heat pump and then to charge the battery. In the area 'b' of Fig. 4, the energy from the PV cannot fulfill the electricity demand. Thus, the battery is discharged to cover the remaining electricity and to run the heat pump. The area 'c' presents how the heat demand is fulfilled if the heat generated from renewables cannot cover it. The highlighted boxes at 'c' and 'd' indicate when the PM is deployed. In PV/battery/heat pump (without PM), these commands are avoided. The last resorts to satisfy the electricity demand is depicted in area 'd'. If the PM is deployed, it is chosen first. Therefore, grid electricity is the last step of EMS. Finally, area 'e' is the last step to fulfill the remaining heat demand using electric heater.

In Fig. 4 the remaining power that needs to be satisfied in the form of electricity or heat is shown with the subscript 'rem'. When the PM is employed and there is no excess electricity from renewables to satisfy the heat demand, the PM is utilized to cover for it. If the heat demand is higher than the nominal heat production of PM ($Q_{\mathrm{rem}} > Q_{\mathrm{PM,max}}$), the engine runs at nominal power. Also the produced electric power from PM is directed to run the heat pump and cover for the remaining heat. Any excess electrical power from PM after the fulfillment of heat demand it first covers the electric demand and then is stored in the bank of batteries.

In the case when there is no excess renewable electricity to satisfy the heat demand but the heat demand is lower than the nominal heat

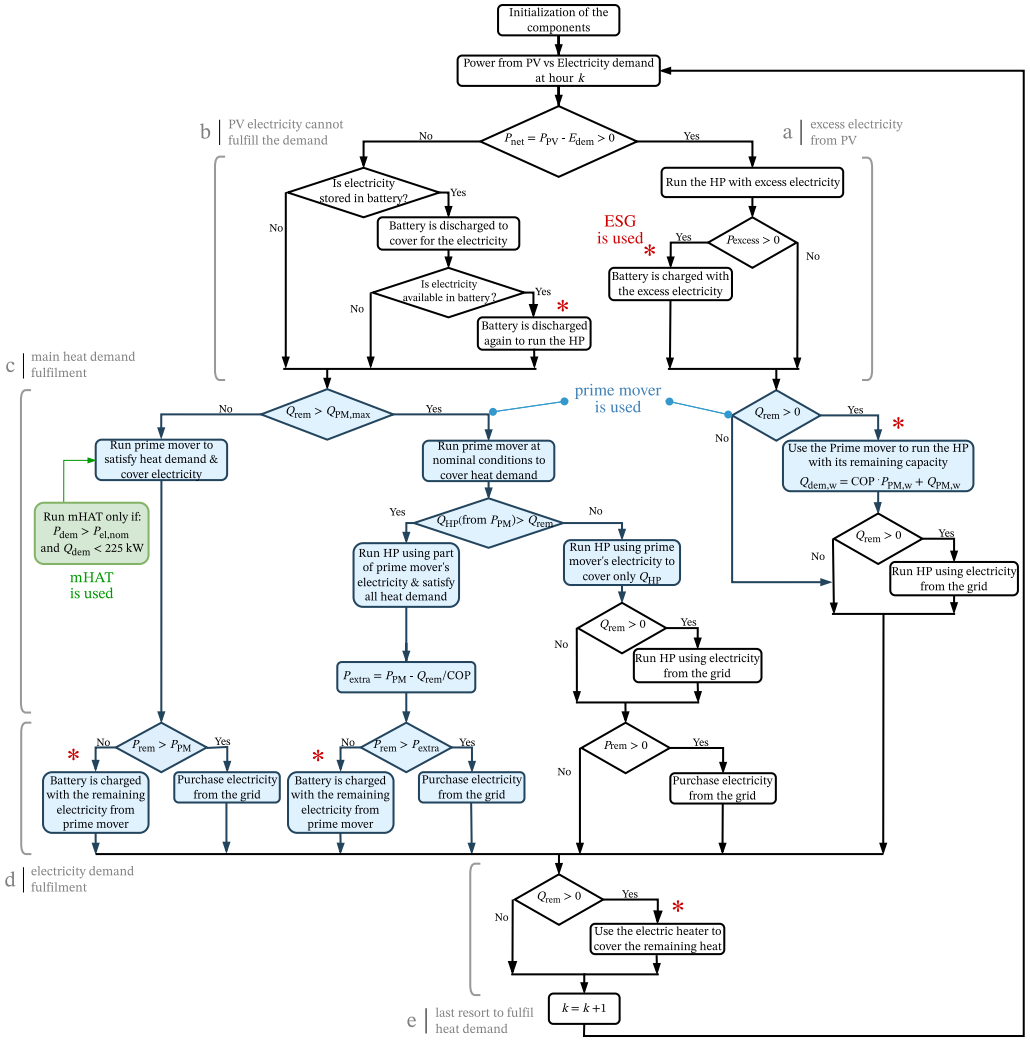

Fig. 4. The flowchart of the energy management strategy for HRES. The commands where the PM is deployed are depicted (PV/battery/heat pump/prime mover). When ESG is commissioned is indicated with an asterisk.

production of PM ($Q_{rem} \leq Q_{PM,max}$), the PM runs on part-load to cover the heat. The electricity that is produced first covers the electricity demand and then is stored in the battery. In this specific occasion that $Q_{rem} \leq Q_{PM,max}$, a green box in Fig. 4 indicates the use of mHAT. Therefore, in the design of PV/battery/heat pump/mHAT, the mHAT engine is used in wet mode when the heat demand is lower than 225 kW_{th} and the electricity demand is higher than the nominal. More information for this specific decision regarding the utilization of mHAT is provided in the next sections.

In Fig. 4, we also indicated when the electrical steam generator (ESG) is deployed to cover for the steam demand only in the hospital case. This is shown with the asterisk (*). Therefore, the algorithm uses the steam generator whenever there is excess electrical power from renewables or prime mover and after the heat pump is deployed. Furthermore, the steam generator fulfills the steam demand in area 'c' using electricity from the grid as a last resort.

Two different examples of the operation of EMS with zero battery capacity are presented in Fig. 5 to assist with the comprehension of the EMS of this study. The arrows of Fig. 5 indicate each step of the algorithm. Example (i) presents a case that produced electricity from PV satisfies all the electricity demand. The remaining electric power from renewables is used by the heat pump to cover for 17% of heat demand (Step 1 in Fig. 5(i)). Then the PM is operated and works at nominal thermal power to cover 19% of heat demand (Step 2). All the

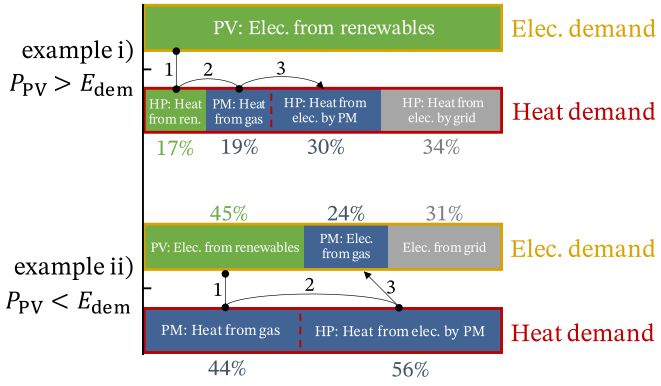

Fig. 5. The two examples on the operation of EMS show how the renewables are prioritized. The PM works to satisfy firstly the heat demand and the grid is the last resort.

electricity produced by the PM is used to run the heat pump and cover 30% of thermal demand (Step 3). The remaining heat is satisfied with the heat pump using electricity from the grid. Example (ii) shows a case where the power from PV covers 45% of the total electricity demand.

At a next step, the PM is used to cover 44% of heat demand. Also, the remaining heat demand is covered by the produced electric power of PM which is used to run the heat pump. In a third step, the extra produced electric power covers 24% of electric demand. The 31% of required electricity is satisfied by the grid.

2.2.1. Solar photovoltaic plant

The PV model follows the implementation described in Coppitters et al. [40], which applies the PVLib framework [41] together with the single-diode formulation and parameter extraction method of De Soto et al. [42]. Therefore, the PV current and voltage are described by a single-diode model equation:

$$I_{PV} = I_L - I_0 \left[\exp\left(\frac{U + I R_s}{n_{diode} N_S U_{th}} \right) - 1 \right] - \frac{U + I R_s}{R_{sh}} \tag{3}$$

A Sunpower SPR X-19-240-BLK module is used as Ref. [43], and Maximum Power Point Tracking is assumed at each time step. Inverter replacement is included using a 10-year lifetime based on reported ranges [44,45].

2.2.2. Bank of batteries

The battery model follows the lead–acid formulation described by Coppitters et al. [40], which builds on the experimentally validated approach of Blaifi et al. [46] for the relationship fo voltage and current:

$$U_{bat} = U_{bat,oc} + I_{bat} R_{bat}, \tag{4}$$

the battery current, denoted as I_{bat}, has positive values when charging and negative values during discharge. The resistance, R_{bat}, influences the voltage changes that occur after both the charging and discharging processes. State-of-charge evolution, current limits, and lifetime estimation through Rainflow cycle counting are treated as in the referenced work, with a minimum SOC of 20% and current constraints based on [47]. The equation of the SOC is shown below:

$$SOC(t) = SOC_0 + \frac{1}{C(t)} \int_0^t \eta_{bat}(t) I(t) dt \tag{5}$$

An initial number of 1250 cycles is adopted in line with previous studies [40]. Further model details are available in [40,46]. Further technical details are provided by Blaifi et al. [46] and Coppitters et al. [40].

2.2.3. Air-source heat pump

The model incorporates inverter heat pump technology. A heat pump that uses ambient air as a source is chosen in this study. The output temperature of the heat pump (T_w) is set at 50 °C (heat sink temperature) and is adopted with the assumption of large area radiators used for commercial building [48]. The hourly operational coefficient of performance is calculated as follows [48]:

$$COP = 6.81 - 0.121\Delta T + 0.000630\Delta T^2, \tag{6}$$

ΔT is equal to $T_w - T_{amb}$, where T_w is the temperature of the heat sink and T_{amb} is the ambient air temperature. The range of operation of this equation is $15 \leq \Delta T \leq 60$.

2.2.4. Prime movers

Four prime movers are evaluated. The mGT configurations in Fig. 6 are compared with an ICE sized to the same electrical load. The optimized layouts include the dry 2-spool mGT and two humidified variants, mGT-wet and mHAT. The dry cycle (Fig. 6(a)) is a 2-spool recuperated and intercooled mGT with an economizer for district heating. The engine model is based on the Aurelia A400 and follows earlier work [49]. Both intercooler and economizer supply hot water at a return temperature of 40 °C, so their cold-side inlet is fixed at 50 °C [50].

Water-injection configurations follow the previously developed models of the 2-spool mGT [51]. In mGT-wet (Fig. 6(b)), preheated liquid water is injected at the HPC outlet, using part of the intercooler flow. The injection rate is limited to avoid two-phase conditions. This concept offers a moderate efficiency gain of about 1%–2% points [51] while using the intercooler and economizer heat at lower outlet temperatures than in the dry cycle.

The mHAT configuration (Fig. 6(c)) saturates the HPC-outlet air through a humidification tower. It provides the highest efficiency improvement without two-phase flow and requires fewer modifications than other humidified cycles [51]. Unlike the HAT cycle [52], no aftercooler is added. Water streams from the intercooler and economizer are mixed, conditioned to meet the thermal demand, and supplied to the saturator. The recirculated water is then split to recover heat from both heat exchangers.

Dry mGT and ICE. Although the prime movers are compared at equal nominal electrical capacity, differences in operational flexibility and part load behavior are explicitly included through technology specific performance curves. Firstly, the dry mGT and ICE and their load curves are presented. Both engines' nominal electrical output is 400 kW_e. The load curves of the intercooled and recuperated dry mGT are produced by the python model that is developed in previous study [49]. The ICE electrical efficiency curve is taken from Tilocca et al. [53] corresponding to a 400 kW_e machine. The thermal output curve is derived from the engines of 2G Energy AG according to 2G Agenitor 406 and Avus 500plus and scaled to match an electrical load of 400 kW_e [54].

The number of units for both PM is also a parameter in the simulation. Therefore, the electrical efficiency is optimized for 2 and 3 units according to the following equation:

$$\eta_{el} = \frac{\sum_{i=1}^{n} P_{el,i}}{\sum_{i=1}^{n} \frac{P_{el,i}}{\eta_{el,i}}}, \tag{7}$$

where n is the number of units and $P_{el,i}, \eta_{el,i}$ the electrical output and efficiency of a single unit. $P_{el,i}$ are the variables and the objective is to maximize electrical efficiency (η_{el}) of the combined engines. Fig. 7 shows the efficiency and thermal power curves versus the electrical power output percentage in case one, two, or three engines are commissioned for the mGT and ICE. Finally, the lifetime of both prime movers is assumed to be 60 000 h which is considered a conservative (relatively high) value [55].

mGT-wet and mHAT. The load curves of the mGT-wet represent the cycle with liquid preheated water injection from the intercooler. The electrical efficiency and nominal load is increased by 1.05% compared to the dry mGT. Although, the produced heat in the form of hot water drops by 32.7% from the dry mGT. The mGT-wet cycle is used only until 150 kW_e of electrical load (37.5% of nominal operation) because at lower loads the efficiency gain is diminished. Thus, below 37.5% of electrical power the dry mGT is employed. This is also depicted with a slight increase in the thermal power output curve of Fig. 8.

The mHAT cycle also operated in two modes. The mHAT presents high exergy efficiency at low heat demands if it is operated with variable thermal demand and nominal electrical output. Fig. 9 illustrates the exergy efficiency and electrical efficiency of the mHAT and mGT. For heat demands below, 225 kW_{th} the mHAT shows higher exergetic performance. As a result, a decision is made to run the mHAT configuration in wet mode only for heat demands for 0 to 225 kW_{th} and for the rest the dry mGT is employed. As it is depicted in Fig. 9 the mHAT at wet mode presents higher electrical efficiency than the dry mGT and constant electrical power at 400 kW_e.

For the CAPEX and OPEX of the mHAT, we assumed that they experience a 10% increase from the dry mGT values. This is considered a conservative assumption [55]. For the mGT-wet a 5% increase is implemented only in the OPEX as it is related with the consumption of water.

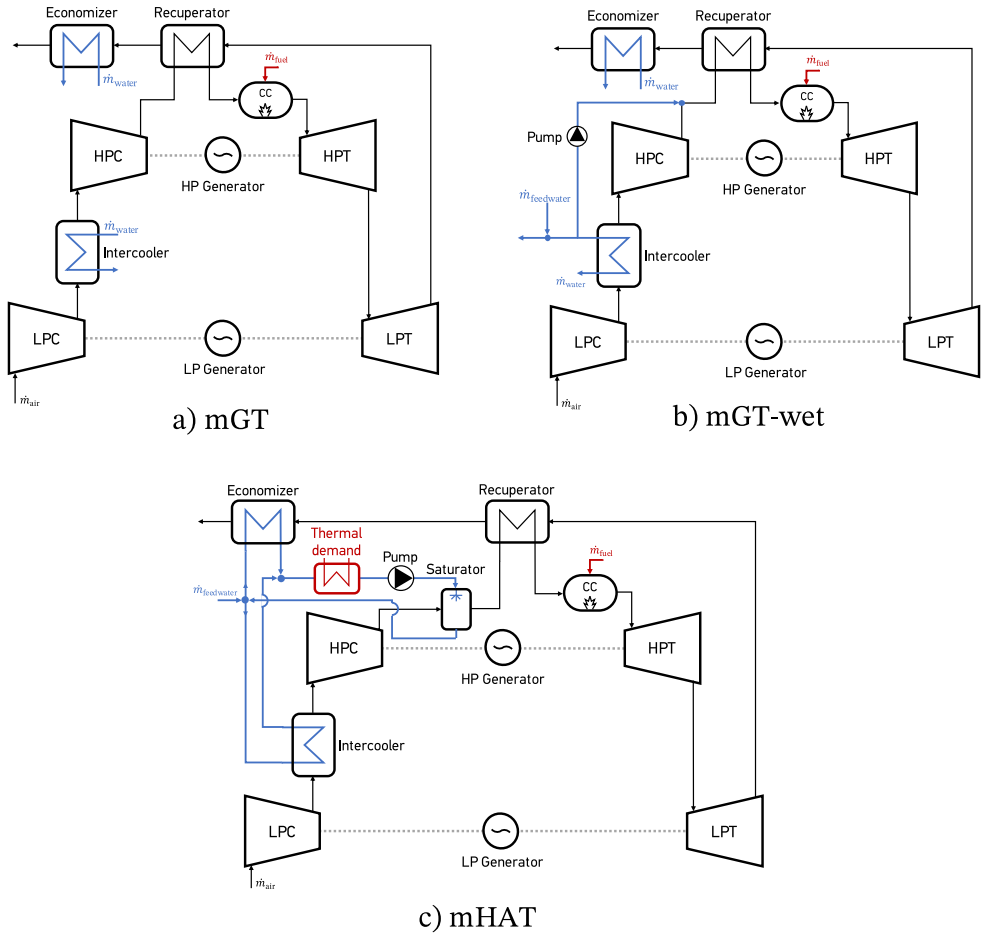

Fig. 6. The dry mGT (a) is compared with a cycle incorporating liquid water injection (mGT-wet (b)) and with the mHAT (c).

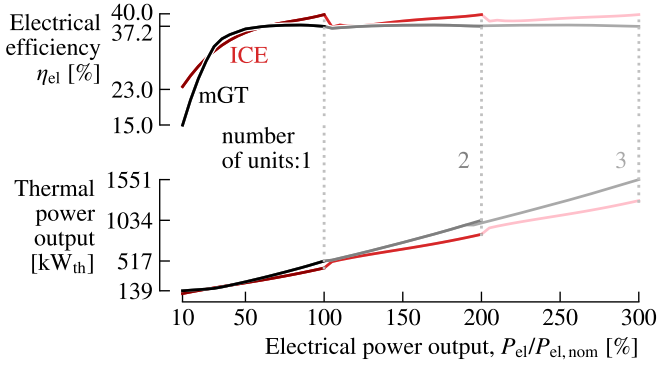

Fig. 7. Electrical efficiency and thermal power output as a function of the relative electrical power output. As the number of units exceeds one, the mGT keeps a rather constant efficiency near the maximum value for more than 75%.

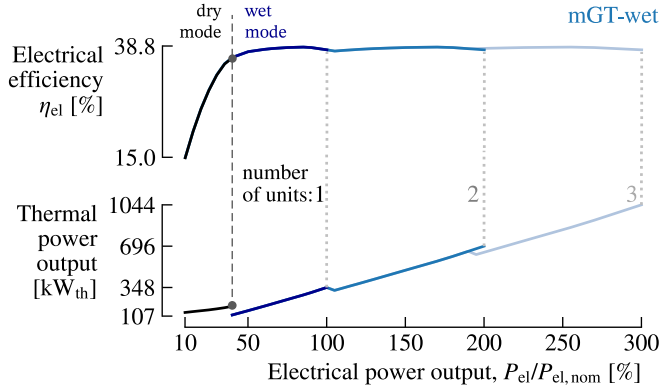

Fig. 8. Electrical efficiency and thermal power output as a function of the electrical power output for the mGT-wet cycle. Higher electrical efficiencies and lower heat loads compared to dry mGT are observed.

2.2.5. *Prime mover for steam generation in hospital*

As it was mentioned in previous section, the hospital requires saturated steam for sterilization and laundry purposes [20,37]. So except for the use of an electrical steam generator, the prime mover is utilized, taking advantage of its hot exhaust gases to generate steam. Thus, for the mGT a heat recover steam generator (HRSG) is placed in the recuperator outlet, as it is depicted in Fig. 10. Basically, the economizer component that generates hot water is in between the HRSG evaporator and preheater to create an effective heat recovery.

Water enters the preheater at 15 °C and 2.04 bar and leaves the evaporator as saturated steam at 120 °C, as it is indicated in global literature of steam generation in hospitals [56–60]. Therefore, the exhaust gases after in the recuperator outlet first use their heat to evaporate the water in HRSG, then heat the water used for district heating and as a last step preheat the water intended for HRSG. The dry mGT is used at nominal electrical load to generate the composite curves of the heat-exchanger network comprised of an economizer and a HRSG. The temperature of flues gases in the recuperator outlet is reported 197 °C. Also, a minimum pinch is applied at the evaporator and preheater of

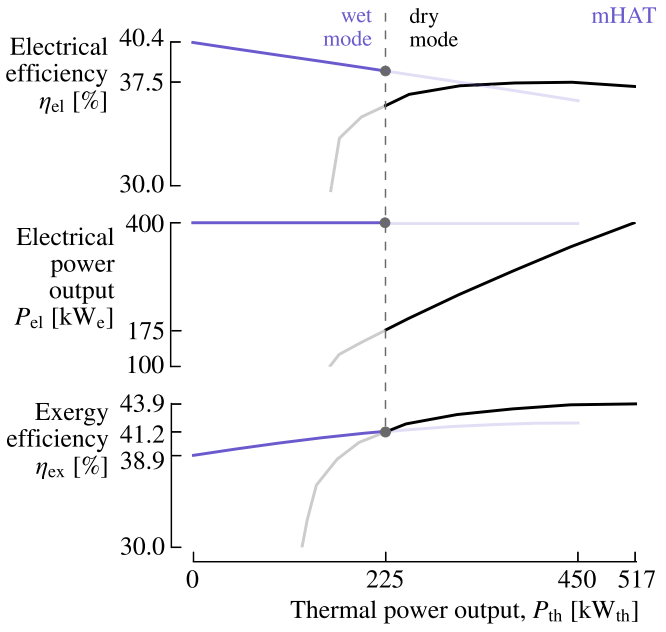

Fig. 9. The mHAT configuration applies water injection through the saturator for thermal power at which the exergy efficiency is higher than the dry mGT. For the rest of thermal demands, the dry mGT is employed.

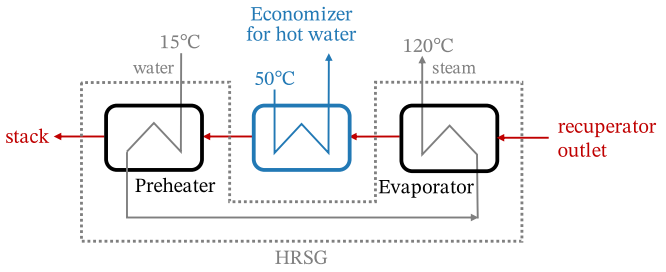

Fig. 10. The HRSG consists of a preheater and an evaporator. The economizer for hot water is placed in between. Saturated steam leaves the HRSG at 120 °C and 2 bar.

10 °C. The economizer is assumed to be unmodified and is modeled with ϵ – NTU method and the off-design behavior is modeled according to Hampel et al. [61]. Fig. 11 depicts the composite curves of the heat-exchanger network for waste heat recovery. The flue gases leave the HRSG at 55 °C. The water used in the HRSG enters the preheater at 15 °C and leaves at 50 °C to be redirected in the evaporator. The water for district heating enters the economizer at 50 °C and leaves at 77 °C. The preheater has a very small effect in the processed heat, taking only 10 kW_{th} from the exhaust gases. Also 180 kW_{th} of heat are processed in the evaporator. As a result, this mGT cycle configuration with a HRSG produces 190 kW_{th} of saturated steam and 357 kW_{th} of water from the intercooler and economizer. The total heat production is, 547 kW_{th} which is increased by 30 kW_{th} compared to the configuration without the HRSG, as a more effective heat extraction is designed. So the steam production is 34% of the total heat of the mGT cycle. The heat transfer equations at off-design in the evaporator are modeled according to Li et al. [62].

For this study, the steam is generated only at nominal conditions. So steam is generated whenever the heat demand is higher or equal than the nominal heat of the prime mover. This design choice is made to reduce the complexity of the calculations. Also, in lower heat loads in the prime mover, the temperature of the exhaust gases drops below 198 °C. As a result, the production of saturated steam is impossible.

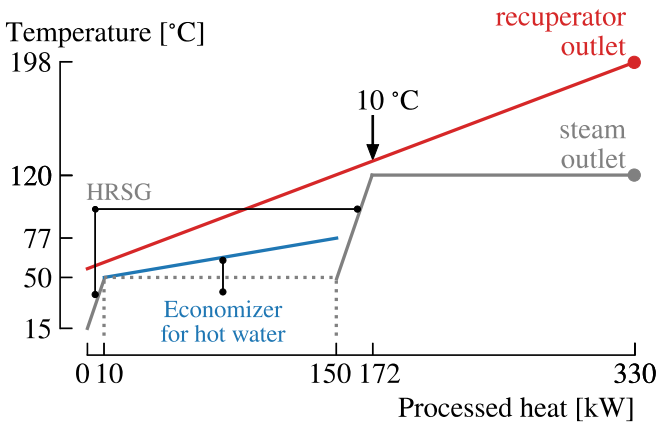

Fig. 11. The composite curves for the HRSG and economizer are designed with a minimum pinch of 10 °C.

Regarding the ICE, it was assumed that this engine produces steam similarly to allow a fair comparison with mGT. Thus, the steam production is assumed to be 34% for the ICE as well. In the mGT-wet the steam production is avoided due to low temperatures at the exhaust (148 °C). Moreover, as the mHAT is operated in dry and wet modes, steam is generated at nominal heat load at dry mode.

2.3. Economic model, optimization and uncertainties

The study designs the HRES system by determining the size of its components, such as the PV array, battery and heat pump, considering them as independent design parameters. The multi-objective optimization is performed using the Non-Dominated Sorting Genetic Algorithm II (NSGA-II) within the RHEIA framework developed by Coppitters et al. [63]. This algorithm is chosen due to the system's intricate and nonlinear characteristics. The optimization algorithm can choose to omit certain technologies, forcing their capacities to be zero. There are two quantities of interest: the Levelized Cost of eXergy (LCOX) and Self-sufficiency ratio (SSR). Other technical and social indicators are not included in the present optimization in order to maintain focus on the economic viability of prime movers in commercial HRES. Therefore, the multi-objective optimization problem is defined as:

$$\min_{\mathbf{x}} \quad F(\mathbf{x}) = [\mathrm{LCOX}(\mathbf{x}), -\mathrm{SSR}(\mathbf{x})], \tag{8}$$

with decision vector:

$$\mathbf{x} = \left[P_{PV},\ E_{bat},\ Q_{HP},\ n_{PM}\right], \tag{9}$$

where: P_{PV} is the installed photovoltaic capacity [kW_p], E_{bat} is the battery storage capacity [kWh], Q_{HP} is the nominal heat pump capacity [kW_{th}], n_{PM} is the number of prime mover units. Symbol i indicates the building type of the 3 cases.

Subject to the following bounds:

$$0 \le P_{PV} \le P_{PV,max,i}$$

$$0 \le E_{bat} \le E_{bat,max,i}$$

$$0 \le Q_{HP} \le Q_{HP,max,i}$$

$$n_{PM} \in \{0, 1, 2, 3\}$$

The LCOX accounts for the true quality of both energy (electricity and heat) streams in the system and is calculated as the total system cost per unit of exergy covered. The self-sufficiency ratio is used as an indicator of the extent to which the system meets its electrical demand without importing electricity from the grid over the year. In this study,

it serves as a proxy for grid dependence under varying electricity price conditions. They are defined as:

$$\mathrm{LCOX} = \frac{\mathrm{CAPEX_a} + \mathrm{OPEX_a} + C_{\mathrm{r,a}} + C_{\mathrm{e,a}} + C_{\mathrm{g,a}}}{X_{\mathrm{demand}}}, \tag{10}$$

$$\mathrm{SSR} = \left(1 - \frac{E_{\mathrm{grid}}}{E_{\mathrm{load}}}\right) \times 100\%, \tag{11}$$

where $\mathrm{CAPEX_a}$, $\mathrm{OPEX_a}$ are the annualized investment and operational cost accordingly; $C_{\mathrm{r,a}}$ is the replacement cost; $C_{\mathrm{e,a}}$ is the grid electricity cost; and $C_{\mathrm{g,a}}$ is the gas cost when a prime mover is considered. E_{grid}, E_{load} are the annual electricity provided by the grid and consumed by the building, respectively. The annualized capital expenses for each system component, represented as $\mathrm{CAPEX_a}$, are calculated as follows [64]:

$$\mathrm{CAPEX_a} = \mathrm{CRF} \sum_{k=0}^{c} N_k \mathrm{CAPEX}_k, \tag{12}$$

where c refers to the different components (e.g., PV, battery bank, heat pump, prime mover, DC/DC converters, and DC/AC inverter) and N represents the corresponding installed capacity. The Capital Recovery Factor (CRF) is determined using the annualized interest rate i and the system lifetime L (20 years) [65]:

$$\mathrm{CRF} = \frac{i(1+i)^L}{(1+i)^L - 1}. \tag{13}$$

The system lifetime is typically chosen as a standard time horizon over which the performance and costs of the entire system are evaluated. This includes factors such as capital expenses, operational costs, and payback periods. In this case, the system lifetime is 20 years, which is common for energy systems like photovoltaic systems or other renewable energy setups. The annualized interest rate i is adjusted for inflation f from the initial interest rate i' at the moment of the loan:

$$i = \frac{i' - f}{1 + f}. \tag{14}$$

This formula is derived from the Fisher equation and allows converting the initial interest rate i' (which does not account for inflation) into the real interest rate, which reflects the purchasing power of money by considering inflation. It allows investors and borrowers to utilize the true cost or benefit of an investment or loan after considering inflation.

System components have different lifetimes, necessitating replacements during the system's operational life, which creates additional costs. The annualized replacement cost is described as [64]:

$$C_{\mathrm{r,a}} = \mathrm{CRF} \sum_{k=0}^{c} \left(N_k R_{c,k} \sum_{l=0}^{r_k} (1+i)^{-t_{rk}} \right), \tag{15}$$

where r_k is the number of replacements during the system lifetime for each component, t_{rk} is the replacement period and $R_{c,k}$ is the future cost of replacement which is assumed to be equal to the CAPEX of the component.

The annual exergy output X_{demand} is characterized by the sum of the annual exergy required for electricity (E), space heating (H), and steam (S) [40]:

$$\sum_{i=1}^{8760} \sum_{\mathrm{type}} X_{\mathrm{type}}^{\mathrm{type}}, \quad \mathrm{type} \in \{\mathrm{E}, \mathrm{H}, \mathrm{S}\}. \tag{16}$$

While the electricity demand is met by the highest energy quality, the exergy required for H and S demand is scaled by their corresponding Carnot coefficient F [40]:

$$X_{\mathrm{type}} = F_{\mathrm{type}} E_{\mathrm{type}}, \quad \mathrm{type} \in \{\mathrm{H}, \mathrm{S}\}, \tag{17}$$

$$F = 1 - \frac{T_{\mathrm{ref}}}{T_{\mathrm{req}}}, \tag{18}$$

where the reference temperature T_{ref} corresponds to the ambient temperature for each specific hour of the year, and T_{req} corresponds to the temperature required for H and S, set at 50 °C and 120 °C, respectively [35,59].

The electricity and gas prices are considered uncertain. Therefore, in this paragraph, the consideration of their mean values is discussed. The electricity price is modeled as a function of time. The electricity prices in Belgium for businesses at each quarter of the year are taken from the Global Petrol Prices database [66]. A linear interpolation between these values is performed to get the electricity cost at every hour of the year. The range of electricity costs throughout the year is between 151 €/MWh and 305 €/MWh. Also, the price for selling the excess electricity back to the grid is considered zero. This approach is adopted to preserve result generality and avoid reliance on location specific regulatory schemes. Given the increasing occurrence of low or negative electricity prices under high renewable penetration, exported electricity often carries limited economic value. This assumption therefore introduces a conservative bias against PV intensive and high self sufficiency designs, emphasizing system performance driven by on site energy utilization rather than market dependent revenues. A feed-in compensation approach and additional streams of revenue for services to the grid should be investigated in future studies. The system utilizes natural gas when the PM is considered. The gas price is taken from the same database as the electricity price, and it is considered uncertain, with a mean value of 82 €/MWh [66].

In this study, uncertainty quantification (UQ) is performed using the approach of non-intrusive PCE, utilizing the framework developed by Coppitters et al. [63]. PCE facilitates the creation of a surrogate model that approximates the actual system response. This model is constructed from a series of orthogonal polynomials whose coefficients are quantified based on the actual model's output. Once these coefficients are determined, analytical post-processing allows for the extraction of the statistical moments (mean and standard deviation) and the Sobol' indices. The standard deviation quantifies the overall variability of the performance metrics induced by uncertain inputs, while the Sobol' sensitivity indices identify the relative contribution of each uncertain parameter to this variability. These indices are instrumental in evaluating the impact of each uncertain parameter on the overall variance of the target metric. For further information, readers are directed to the referenced work by Coppitters et al. [63]. So, in this work, robustness refers to the sensitivity of the optimized system performance to uncertain input parameters. A design is considered robust when it exhibits a low standard deviation of LCOX under uncertainty propagation, indicating limited performance variability despite fluctuations in economic and climatic inputs. Robustness is therefore assessed on Pareto-optimal solutions and is not related to control stability or fault tolerance.

Table A.1 shows the mean and standard deviation for various climate (solar irradiance, ambient temperature), economic (CAPEX, OPEX, electricity and gas prices), and design conditions ($\eta_{\mathrm{DC/DC}}$, $\eta_{\mathrm{DC/AC}}$, $\mathrm{COP_{HP}}$) with their corresponding references. The UQ is performed on the Pareto fronts that are calculated with NSGA-II.

The computational budget and population size are fixed by the user in the NSGA-II optimization. Therefore, the population size is 30 to ensure a sufficient exploration of the design space. The number of CPU cores that are utilized is 24 and the number of generations is initially set at 250 for an effective exploitation. Each generation had a duration of approximately 17 sec and 250 generations lasted ~71 min (duration of optimization). After the completion of 250 generation, the optimization continued to smoothen the Pareto fronts and the design variable curves. All those parameters are determined based on the indications of the documentation of RHEIA framework [63].

UQ is then applied a posteriori to the Pareto-optimal solutions obtained from the deterministic NSGA-II optimization. The PCE-based analysis is therefore carried out exclusively on optimized system designs, with the objective of assessing their stochastic performance in terms of LCOX and self-sufficiency, as well as identifying the dominant sources of uncertainty through global sensitivity analysis.

Table 2
A limit on the capacity of PV is introduced for the three studies based on the area of the rooftops.

case	roof area [m^2]	max PV capacity [kW_p]
hospital	22 400	2160
office	46 300	4460
hotel	11 350	1095

3. Results and discussion

This section is divided into three subsections. At first, the case of the hospital, then the case of the office building and at last the case of the hotel are presented. In all case studies, the results of multi-objective optimization regarding the LCOX and SSR are presented with the Pareto fronts. The results of the HRES without PM are compared with those when mGT and ICE are included into the system with a fixed capacity.

Based on market analysis, to keep realistic component sizes in commercial building, the design space of the parameters is constructed. Thus, the upper limit for battery and heat pump capacities is 18 000 kWh and 9000 kW_{th}, respectively. More specifically, regarding the battery upper limit, further increase has minimum effect on the SSR and increases dramatically the LCOX. The PV capacity upper limit had also to be defined in this study. In this analysis, we assume that the floor area for each building taken from Open Energy Information's [35] corresponds to the roof area. So, it is estimated that half of this area is effectively used for PV panel installation, which is an optimistic approach according to Ghaleb et al. [67]. As a result, the maximum PV capacity for the three case studies is presented in Table 2. The imposed PV area constraint reflects practical architectural limitations and avoids overestimating the contribution of on-site solar generation.

3.1. Hospital

3.1.1. Multi-objective optimization

The HRES layouts with a commissioned prime mover achieve lower LCOX than the PV/battery/heat-pump case (see Fig. 12). The Pareto fronts show the trade-off between LCOX and SSR for the dry mGT, mGT-wet, mHAT, ICE and the configuration without a prime mover. Uncertainty bands indicate the range of outcomes for the mGT, ICE and the no-PM case (1 std). Across all options, the SSR remains limited to about 30%, driven by the PV capacity constraint and the EMS logic described in the next paragraphs.

The configuration without PM presents an LCOX of 244 €/MWh at the lowest SSR (28.1%). The cases in which a PM is commissioned (mGT, ICE) show lower LCOX in their lowest SSR. The configuration of mGT has an LCOX of 226.9 €/MWh and the ICE case 227.3 €/MWh. Therefore, it is revealed that in the hospital case, the system becomes more cost-effective as a PM is used. More precisely, the mGT case depicts the lowest cost of exergy production. The global sensitivity analysis in all three configurations presents the lowest standard deviation in the lowest average LCOX. The case of ICE shows the most robustness at that point with a standard deviation of 11.8 €/MWh, closely followed by the mGT (11.97 €/MWh) and the case without PM (12.47 €/MWh). Also, all cases have the maximum standard deviation at maximum SSR, around 18–19 €/MWh.

As the installed capacity increases, the SSR rises only slightly (from about 28% to 30%), while the LCOX increases significantly (from about 227 to 336 €/MWh in the mGT case), and the lowest average LCOX corresponds to the most robust design. Therefore, the lowest average LCOX is chosen for the optimum designs for all cases (see the circles in Fig. 12). To explain the shape of the Pareto fronts of Fig. 12, it is necessary to present how the design variables (components capacities) evolve with respect to LCOX.

Fig. 13 presents the capacities calculated from NSGA-II to illustrate the Pareto fronts for the cases with and without PM. The PV

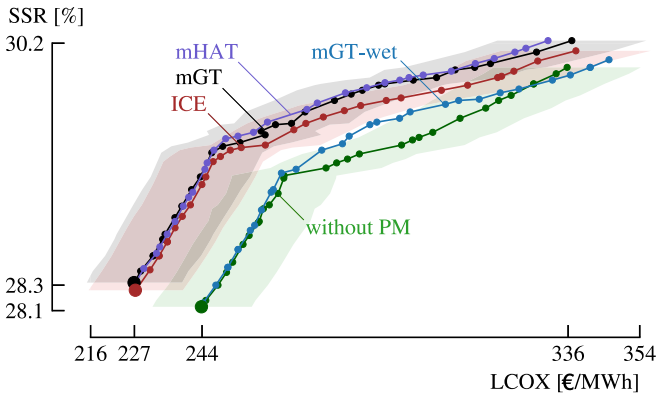

Fig. 12. The Pareto fronts between minimizing the LCOX and maximizing the SSR as five different technologies are considered in the hospital case. The UQ revealed that the most robust design is presented in the lowest mean LCOX. In the most robust designs, the LCOX is lower for the configurations that consider a PM. This is linked with the high heat demand which is presented in the hospital.

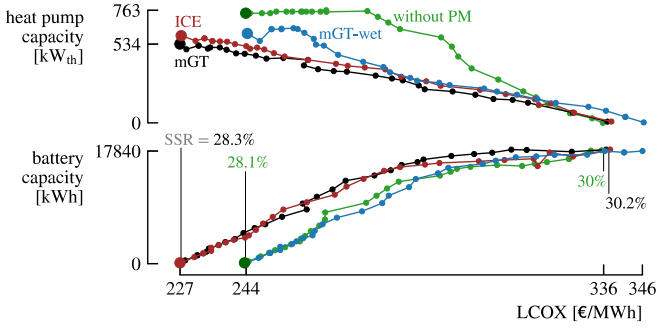

Fig. 13. Battery and heat pump capacities with respect to the LCOX with and without PM. The lowest LCOX is observed without the use of batteries. The highest LCOX is shown without heat pump. The mHAT system is avoided because it exhibits behavior similar to that of the mGT.

capacity is not depicted as it reaches a maximum (2160 kW_p) for all configurations. Fig. 13 shows that as the battery capacity rises and reaches a plateau, the LCOX increases significantly for all cases. The opposite behavior is shown for the heat pump capacity. So the heat pump size decreases from 763 kW_{th} in the case without PM and from 534 kW_{th} in the mGT case, to zero. As we move up in the Pareto front, the gain in SSR is very small compared to the LCOX penalty. Thus, the selected design point is chosen at the lowest LCOX with also the lowest standard deviation. At the desired design choice, the heat pump capacity is maximum, and the battery capacity is zero. This is a direct product of the EMS. As the electricity demand is satisfied by the PV, the excess energy is directed first to the heat pump to cover the heat demand in district heating, then to the electrical steam generator to cover for the high steam requirement and at last to the battery. As a result, at the lowest LCOX, the heat pump capacity is the highest, and there is limited excess electricity to be stored in the battery. The LCOX increases as the heat pump capacity decreases. As the heat pump goes to zero, the heat demand is satisfied mostly with the electric heater. As a result, the LCOX is increased dramatically. Also, the battery capacities are increasing with a reducing rate with respect to LCOX at high SSRs, which creates a bending point and linear behavior in the Pareto fronts of the all systems (see Fig. 12).

The LCOX and SSR are increased as the battery capacity rises. The maximum SSR is observed in the designs where the battery capacity is at the maximum and the heat pump capacity is zero. So, all the excess electricity from the PV at first satisfies the ESG and then is stored in the

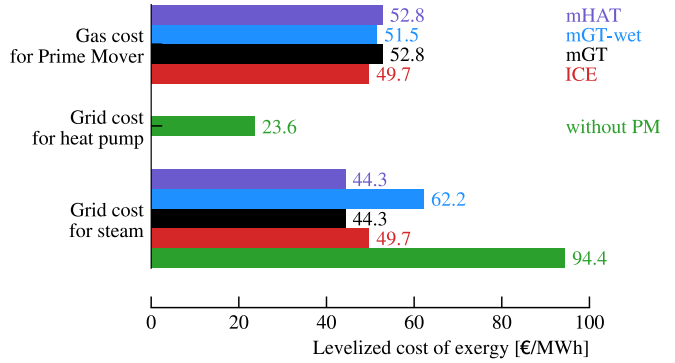

Fig. 14. The combined gas cost and grid cost for steam in mGT and ICE are lower than the combined grid cost for heat pump and for steam in the case without PM.

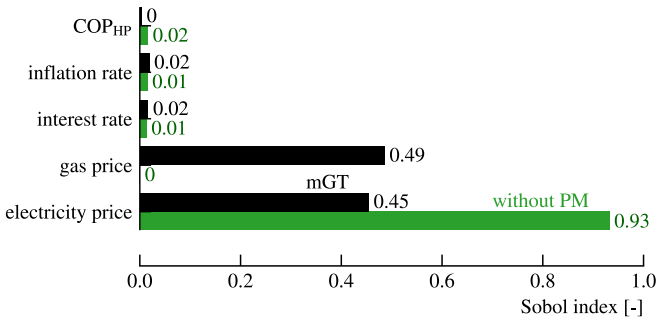

Fig. 15. Top-5 total order Sobol' indices of mGT and without PM. The case without PM is influenced mainly by the electricity price, whereas the mGT by the gas price.

battery. Therefore, the amount of stored energy when the heat pump is not used increases. The behavior of the sizes of heat pump and battery is also a result of the upper limit that is chosen in the PV capacity. A PV capacity that could satisfy the heat demand with the heat pump and electrical steam generator would allow the battery to store more electricity and thus increase the SSR. However, as the upper limit of the PV capacity increases, the simulation becomes less realistic because the available area for PV in a hospital is limited as we chose to utilize only the available area of the building.

Table B.1 and Fig. 14 are used to portray the cost parameters of the optimum designs of different HRES and give a thorough view of the mechanisms affecting the cost. All the component, gas and grid costs are presented divided by the total demand in exergy to show the portions of the total LCOX. Observing the optimum results, the mGT case shows the lowest LCOX and the highest SSR. This is the result mainly of the high demand in steam, which is presented by the highest component cost of ESG and the electricity required from the grid to run the ESG (see "grid cost for steam" in Fig. 14). The mGT presents the lowest grid cost for steam (49.7 €/MWh) as it does not only generate steam with a HRSG at the nominal load but also utilizes part of its produced electric power to run the ESG. Also, the use of PM for the four cases diminishes the need of running the heat pump with electricity from the grid (grid cost for HP is 0.1 €/MWh). So for the case without PM and due to the low SSR, most of the time the produced PV electricity does not fulfill the electric demand and thus limited electricity is offered to run the heat pump and steam generator. This is shown in Table B.1 as the grid electricity for heat production has the highest number (8940 MWh) compared to the other systems.

The mHAT case shows the exact same results as the dry mGT case, except for an increased component cost of PM. This is the result of the demand profile of the hospital. The limitation in the PV capacity coupled with the high heat demand generate a scenario in which the demanded heat is rarely lower than 225 kWh in order to run the mHAT in wet mode. The results show that the wet mode of mHAT is utilized only 0.1% of the year. This indicates that the mHAT is not suitable for buildings with high heat requirements.

The mGT-wet shows the worst LCOX in this case. This is associated with its inability to produce steam with a HRSG. Fig. 14 shows that the grid cost for steam is increased compared to the other PM cases. Also, the cost of steam generator is elevated. However, this system uses the generated electric power of the mGT-wet to run the heat pump and steam generator, thus decreasing the grid electricity for heat compared to the case without PM. This behavior allows it to present comparable LCOX as the system with the employment of PM.

The ICE shows comparable results with the mGT system, as it presents a LCOX increased by 1.2 €/MWh and an overlap in the confidence interval. The ICE has higher requirements of grid electricity for heat. As the grid cost for steam is increased as well, this indicates that the lower heat production of the ICE is the reason behind the higher LCOX. Therefore, the lower CAPEX and higher efficiency of this ICE compensates for the higher grid requirements for steam generation, placing this system closely to the mGT in terms of LCOX.

3.1.2. Global sensitivity analysis

A global sensitivity analysis is performed on the optimized designs of Fig. 12 to determine the main drivers of the LCOX. Thus, in the selected optimum designs (see the circles of Fig. 12), the Sobol' indices are depicted for the case without PM and the mGT case. The other PM cases are not presented as they show similar results to the mGT. Fig. 15 presents the top-5 total order Sobol' indices for the two cases. The main driver for the variability of the LCOX in the configuration without PM is the electricity price. This is because the heat pump and steam generator usually run with grid electricity to satisfy the heat demand. The LCOX of the mGT case is influenced mainly by the gas price, with a Sobol' index of 0.49, followed by the electricity price, with an index of 0.45. In this case, the fuel is used to run the PM and together with the heat pump, they cover the heat demand. Consequently, the gas price has the most important role in the variability of the LCOX. In the mGT case, the second place belongs to the electricity price, as the system consumes 11.4 GWh from the grid during the year to cover the remaining heat and electricity. In both cases, there are small influences from the inflation and interest rate. Also, the uncertainty in the COP of the heat pump affects slightly the LCOX behavior due to the high capacity of this component in the optimum design.

These results indicate that the increased LCOX in the HRES without PM compared to the mGT and ICE is associated with electricity and gas prices. As the electricity price in Belgium is more than double the gas price during the year [66], it is cheaper to use a PM together with heat pump to cover the heat demand. This claim is confirmed by increasing the gas price in the mGT case and observing the behavior of LCOX. Therefore, if we consider an increased gas price by 50% and advancing it towards the reported prices for e-methane [68,69] the gas cost will be 123 €/MWh and the optimum LCOX is 253 €/MWh. Fig. 16 shows the progress of LCOX as the gas price is increased with a 25% step. Therefore, by the gas price increasing by 33%, the LCOX of mGT case matches the value of the case without PM (244 €/MWh). This means that the mGT system is still competitive against an HRES without PM for prices around 109 €/MWh and average electricity cost 180 €/MWh for this specific case study. Thus, the lowest electricity-to-gas ratio is 1.65. A further increase in electricity price penalizes more the case without PM because this system presents higher Sobol' index compare to the mGT case.

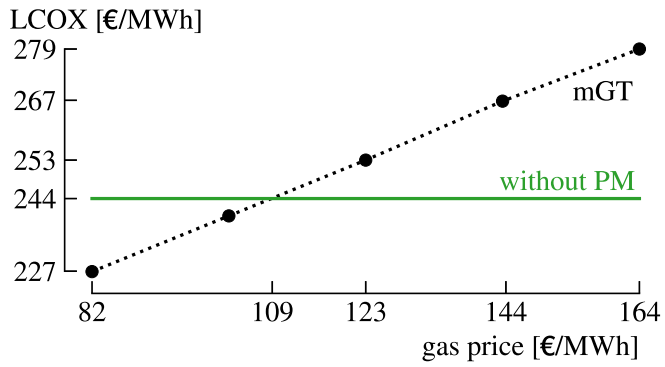

Fig. 16. The LCOX of the mGT system at various gas prices. As the gas price is increased by 33% the mGT system remains competitive again the HRES without prime mover.

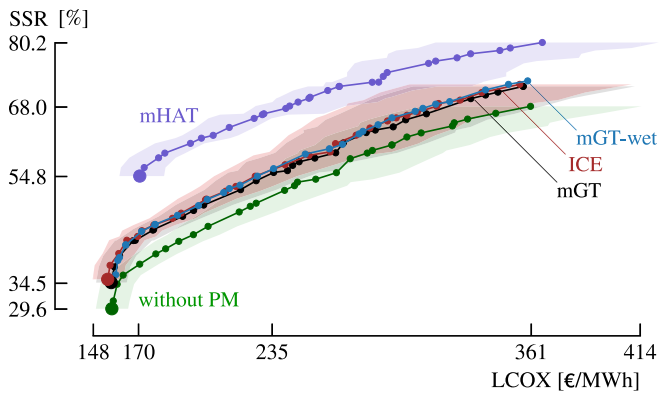

Fig. 17. The Pareto fronts for the 5 HRES shows that the system with the lowest LCOX is the ICE due to the low CAPEX of this prime mover.

Table 3
The LCOX and SSR are shown as the number of mGT units is increased. At 3 units, the prime mover works fewer times at nominal load and less steam is generated from the HRSG, leading to lower SSR compared to 2 units. Thus, the 3-unit case (shown italicized) yields a higher LCOX, not due to the additional unit but due to the EMS configuration, which is not optimized for this layout.

Installed mGTs	LCOX [€/MWh]	SSR [%]
Single unit	227.3	28.3
2 units	214.5	47.5
3 units	*229.9*	*39.26*

3.1.3. SSR vs number of units

As the number of PM units utilized in the HRES is increased, the SSR of the system should be increased. Table 3 presents the optimized LCOX and SSR as the number of units increases. For 2 units, the LCOX is decreased to 214 €/MWh because more heat demand is satisfied from the prime mover and more generated power is used to run the heat pump and steam generator. Also, the SSR jumps to 47.6% as more electrical power that is generated from the prime mover is used to satisfy the electricity requirements. So, the system becomes less dependent on electricity prices and more dependent on gas prices. When 3 units are used, the SSR is 39.26 %, and the LCOX is 229.9 €/MWh. So the SSR is not increasing as initially expected. This indicates that the mGT is operated fewer times at nominal conditions, as a result the HRSG is producing less steam compared to 2 units. The grid cost for steam is 6 and 32 €/MWh for 2 and 3 units, respectively. More produced electrical power of the mGT is directed to satisfy the steam demand with ESG, resulting in lower SSR compared to 2 units. Thus, at 3 units, the EMS should be redesigned to account for each time a single unit works at nominal to and utilize the HRSG. However, this requires more complex modeling of the system and prime mover and it is out of the scope of this study.

3.2. Office

3.2.1. Multi-objective optimization

The office case has completely different characteristics of heat and electricity demands than the hospital case. The demand profiles are described thoroughly in the subsection "Climate and demand data" of the "Methodology" section. This case presents low heat demand compared to the electricity required. So, the effect of a PM on the LCOX for such demand profiles is studied. Also, for this case, there are no requirements for steam. In this case, the findings regarding the mHAT are expected to change. This is the only engine that is not heat driven. The other three prime movers are operated only when there is heat demand higher than the minimum generated thermal power (see Fig. 7). However, the mHAT decouples heat and electricity and run at constant electrical power at lower heat demands.

Fig. 17 shows the Pareto fronts for the five considered configurations. All the different HRES show a sufficient range of SSR in the optimal designs. More specifically, the case without PM shows and SSR range from 29.6 % to 68 %. The design with the lowest LCOX (154.9 €/MWh) is shown at SSR = 35.16 % and belongs to the ICE system. The adopted design for each HRES is chosen again at the lowest SSR, regardless of the steep increase of the Pareto front for low SSR and LCOX. This choice is made to ensure that the system with the lowest cost is determined, as the configurations have very close values of LCOX.

As shown in Fig. 17, for both ICE and mGT the LCOX is lower (see the circles of Fig. 17) than the case without PM in the selected design. The mGT shows a LCOX of 156.6 €/MWh and the case without PM 156.9 €/MWh. Also, the mGT, ICE and mGT-wet show rather similar SSR with the mGT-wet to have the highest from the other two. The Pareto front of the mHAT presents increased LCOX (170.5 €/MWh at the selected design) but the highest SSR for all the other systems with same electricity-to-gas ratios (above 2). The lowest standard LCOX deviation for all the systems is shown at the lowest SSR, as in that design the system is more depended on the grid and on the capacity from the battery. The ICE is the most robust with a standard deviation of 7.4 €/MWh. The mGT has a slight higher std at 7.44 €/MWh. The case without PM shows 7.84 €/MWh as it is more influenced from the grid. The highest variability belongs to the mHAT because more fuel is used and thus is more affected by the gas price. This is confirmed by examining the total order Sobol' indices. The mGT case has 0.677 for the electricity price and 0.114 for the gas price. While the mHAT shows 0.154 for the electricity and 0.743 for the gas price. At the highest SSR, the standard deviation of all the systems increases around 54 €/MWh as the Sobol' index for the CAPEX of the bank of batteries jumps to 88%. A detailed analysis on the capacities of the configurations is presented in Appendix C.

The superiority of ICE in terms of cost is driven by its low PM component cost (3.5 €/MWh). The lower grid cost is compensated by the higher gas cost. Thus, the CAPEX of ICE is responsible for the lowest reported LCOX. The mHAT shows decreased grid cost for electricity compared to the other PMs, but the increase in gas cost is higher. The wet mode of the engine is used 40.6% of the year. Therefore, the mHAT only increases the grid independence for this demand profile with higher average electricity than heat. This boost in SSR occurs with a considerable LCOX penalty, however the other PM configurations for the same SSR show a LCOX around 235 €/MWh (see Fig. 17) Therefore at occasions in which the grid independence is necessary, the mHAT offers a very low LCOX penalty.

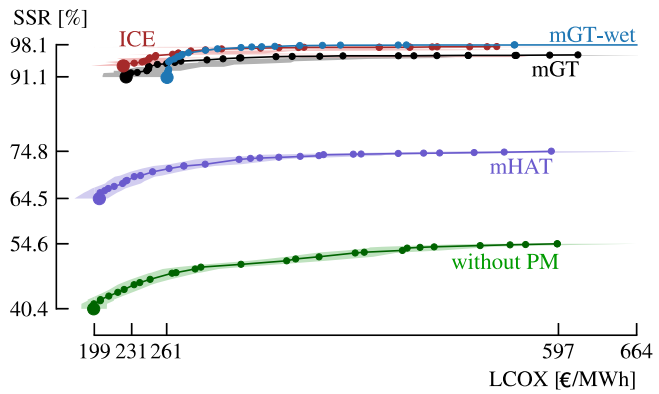

Fig. 18. The Pareto fronts for the 5 HRES shows the superiority of the system without PM. The inclusion of PM lowers capacity from PV and more energy is produced using fuel and increasing the LCOX.

3.2.2. mGT vs ICE

The analysis of the office scenario reveals that the ICE configuration achieves better economic results than the mGT. Therefore, it is interesting to determine the reduction in $CAPEX_{mGT}$ that is needed for the mGT scenario to match the LCOX of the ICE scenario. The calculations indicate that reducing $CAPEX_{mGT}$ by 24% would result in an equivalent LCOX to that of the ICE scenario. This reduction equates to a $CAPEX_{mGT}$ of 873 €/kW_e, which remains 28% above the $CAPEX_{ICE}$.

3.3. Hotel

3.3.1. Multi-objective optimization

The hotel case presents low heat and electricity demand than the other two case studies, with maximum demanded electricity near the nominal power of the prime mover at 422 kW_e. Therefore, it is expected that the inclusion of a prime mover will produce a SSR close to 100%. Fig. 18 shows the Pareto fronts for the different energy systems. The lowest LCOX is depicted at 198.4 €/MWh and it belongs to the HRES without PM. The chosen designs are at the lowest LCOX as with the other cases to assist in the correct comparison of the technologies. This system also has the lowest SSR at 40.4%. The mHAT shows the second lowest LCOX and an SSR in between the other PMs and the case without PM. However, the results of mHAT should be analyzed further to draw any conclusion regarding it effectiveness in the hotel case. The other PMs (ICE, mGT, mGT-wet) show increased LCOX and a Pareto front near 100% self-sufficiency, which confirms our initial predictions. As with the other case, the mGT-wet presents again the highest cost at the optimal point, highlighting that this configuration is not suitable for CHP systems.

The case without PM presents also the lowest standard deviation (11€/MWh) in LCOX from the other cases at the lowest cost. The mGT case is more robust than the ICE as it presents a standard deviation around 25 €/MWh and the ICE 27.5 €/MWh at the lowest LCOX point. The Sobol' indices for the case without PM reveal that this system is mainly influenced by the electricity price with a Sobol' index of 0.63 and by the COP_{HP} with a Sobol' index of 0.15 as the heat pump capacity is the highest in its Pareto front with 951 kW_p. Also, the inflation and interest rate have 0.06 and 0.07 indices respectively. The mGT is significantly influenced by the gas price, with a Sobol' index of 0.71 and comparable values of inflation and interest rate. Also, the mGT shows its dependence with the electricity price by a Sobol' index of 0.1 as a small portion of the demanded electricity is covered from the grid. As with the office case, a detailed analysis on the capacities of the configurations is presented in Appendix C.

The case without PM shows the lowest cost, as the presented grid cost for electricity and HP is 161.5 €/MWh (see Table B.3). This parameter is lower than the gas cost for PM and the grid requirements for the other cases. The ICE and mGT have a grid cost for electricity and gas cost of 180.5 €/MWh and 170.1 €/MWh respectively. Also, the superiority of the case without PM is shown by the energy provided from PV. The electricity by PV is 1170 MWh for this case and around 877–878 MWh for the ICE and mGT. The mGT-wet presents low electricity from PV because its thermal output is lower than the dry mGT for the same electrical power. As the PM systems are heat-driven for the same amount of heat required, the mGT-wet produces more electric power and consumes more fuel. Therefore, lower PV capacity is needed for this case.

As the results of mHAT case are examined, it is shown that the wet mode of the cycle is never utilized by the energy management system. This is because the demanded electric power is never higher or equal than the nominal mGT electricity at that stage (see the green box of Fig. 4). As a result, water injection is never performed. Thus, the results simulate the mGT case but utilized fewer times per year and with a higher CAPEX. If the condition of the demanded electricity (being equal or higher than the nominal) is removed from the energy management system, the optimized LCOX and SSR for the mHAT is calculated to 310.2 €/MWh and 97.5%, respectively. These results confirm the increase in SSR that is expected by running the engine at nominal electric power. However, it is shown that the mHAT case is not suitable in terms of cost to be coupled with PV/batter/heat pump for electricity demands lower than the engine's nominal power.

3.4. Discussion on limitations of EMS and on cost values

The energy management strategy applied in this study follows a fully deterministic, rule based structure. The dispatch logic prioritizes direct use of renewable electricity, then heat pump operation, followed by storage and finally grid import. This structure directly constrains the feasible operating space of the system and therefore shapes the resulting Pareto fronts.

In particular, the limited increase in self sufficiency observed across most Pareto fronts is a direct consequence of the EMS prioritizing heat production over electrical storage. Excess photovoltaic electricity is first allocated to the heat pump and steam generation, which reduces the availability of surplus electricity for battery charging. As a result, increasing battery capacity leads to marginal gains in self sufficiency but a steep increase in the levelized cost of exergy.

The EMS also enforces a standard heat driven operation of the prime movers [28], which limits their use in electricity dominant periods. This structural choice favors solutions with high heat pump capacity and low battery capacity at minimum cost points. Alternative EMS formulations, such as battery first dispatch or power driven prime mover operation, would likely reshape the Pareto fronts and shift the optimal designs. However, such strategies would require a fundamentally different control formulation and are outside the scope of the present work.

Other constraints that could limit the generalization of the results should be stated. Excess electricity exported to the grid is assigned to a zero value, which avoids dependence on location-specific feed-in tariffs but could penalize PV-intensive and high self-sufficiency configurations such as the results of humidified engines. In addition, the photovoltaic capacity is restricted by the available rooftop area of each building, reflecting realistic architectural constraints. This limitation caps the achievable self-sufficiency and directly influences the Pareto fronts and the economic ranking of the optimal designs.

The LCOX values that are calculated in this study are consistent with reported cost levels for hybrid renewable energy systems in the literature. Although several recent works report levelized cost of electricity (LCOE) instead of LCOX, recent analysis on grid-connected PV–battery–hydrogen systems report LCOE values in the range of 269–363 €/MWh [70]. Furthermore, studies including mGTs and ICEs for hydrogen backup applications indicate LCOE values between 800

and 1100 €/MWh [71]. In addition, LCOX-based assessments of hybrid PV–battery–heat pump systems under European conditions report values between 623 and 980 €/MWh [40]. Although direct numerical comparison is limited by differences in performance metrics, system boundaries and demand profiles, these results confirm that the cost levels obtained in this work are of the same order of magnitude. In this context, LCOX is used as a comparative indicator to assess different technologies under identical assumptions rather than as a tool for absolute cost validation.

4. Conclusions

This paper employs design optimization and uncertainty quantification on a system that integrates photovoltaic arrays, battery storage, heat pumps, and two distinct prime movers, ICE and mGT. Targeting a hospital, an office and a hotel located in Brussels, this investigation handles their unique demand profiles. The optimization utilizes two objectives: minimizing the LCOX and increasing the system's SSR. The study's main focus is to compare the optimized designs without PM with those that incorporate PM regarding their calculated LCOX. Also, the economic results of the prime mover cases are compared in an uncertain techno-economic operating environment. The conclusions drawn in this study are specific to the investigated demand profiles, climatic conditions, and design constraints. The case study is limited to buildings located in Brussels, and the photovoltaic capacity is constrained to the available roof area in order to represent a realistic retrofit scenario.

1. Hospital case findings: In the hospital case, integrating a prime mover enhances the cost-effectiveness of the HRES, with the mGT configuration showing the lowest LCOX of 226.9 €/MWh and the highest SSR of 28.3%. The mGT's ability to generate steam and run the heat pump and steam generator with its produced electricity leads to reduced reliance on grid power, lowering the overall cost. The mHAT configuration, although showing similar robustness, is used only 0.1% of the year due to the high heat demand profile (demanded heat rarely less than 225 kW_{th}), making the transformation from mGT to mHAT an unreasonable choice for this case. The mGT-wet, on the other hand, shows the highest LCOX among the PM configurations due to its inability to produce steam with an HRSG, leading to increased grid costs for steam. The ICE configuration, although is close to the mGT in terms of cost, has slightly higher grid requirements for heat. Thus, for hospital application with high steam demand, the mGT system emerges as the most efficient and cost-effective solution. Sensitivity analysis shows that LCOX is mainly driven by electricity prices in systems without PM and by gas prices in mGT systems. PMs with heat pumps remain cost-effective even at high gas prices. Introducing a second prime mover lowers both LCOX and increases SSR. Adding a third unit reduces SSR because it operates more often at part load, indicating that a different EMS strategy would be required for such a configuration.

2. Office case findings: For the office case, the ICE provides the lowest cost, with the mGT close behind. Both perform well because the heat demand is limited and electricity dominates, so electricity production acts as the main driver. The mHAT increases SSR but becomes more expensive due to its higher gas use as the wet mode is used at nominal conditions and no electricity is sold bac to the grid. Similarly, the mGT-wet also raises costs but offers only a small SSR increase.

3. Hotel case findings: For the hotel, the layout without a prime mover results in the lowest LCOX, and adding prime movers increases costs with limited benefit because the average electricity demand is lower than the nominal electric power of the PM.

4. Prime mover role in the HRES: The results show the potential of applying CHP units in buildings with high energy demands, provided that the mix of electricity and gas prices allows such configurations. The use of HRSG is a key parameter for the cost-effectiveness of the PM systems in the hospital case. Also in the office case, the PM systems show exceptional cost-effectiveness on handling intermittent high heat demand. The cases with water injection present higher LCOX compared to the dry mGT in all three cases. However, the mHAT system can be applied if the user's scope is to decrease the influence for the electricity price and redirect it to the gas price.

5. Future perspectives: Future work will extend the present framework toward robust design formulations, in which system sizing decisions are optimized directly under uncertainty. Such an approach would enable the identification of designs that remain robust across a wide range of economic, climatic, and technical conditions. Also, the integration of broader socio economic indicators could further enhance the assessment of system performance. Lastly, the integration of load scheduling in a weak-grid systems could be explored in future extensions of the framework.

CRediT authorship contribution statement

Aggelos Gaitanis: Writing – review & editing, Writing – original draft, Visualization, Resources, Methodology, Investigation, Formal analysis, Data curation, Conceptualization. **Diederik Coppitters:** Writing – review & editing, Software, Methodology. **Ward De Paepe:** Writing – review & editing, Supervision, Funding acquisition. **Francesco Contino:** Writing – review & editing, Supervision, Project administration, Funding acquisition, Conceptualization.

Declaration of competing interest

The authors declare that they have no known competing financial interests or personal relationships that could have appeared to influence the work reported in this paper.

Acknowledgments

Co-funded by the European Union

The authors would like to acknowledge the financial support received from the European Union's Horizon 2020 research and innovation programme under grant agreement No. 861079 (NextMGT — Next Generation of Micro Gas Turbines for High Efficiency, Low Emissions, and Fuel Flexibility). This paper reflects only the authors' view and the Research Executive Agency, and the European Commission are not responsible for any use that may be made of the information it contains. Co-funded by the European Union under PN: 101083536 ("Fit4Micro-Clean and efficient micro CHCP by micro turbine based hybrid systems"). Views and opinions expressed are however those of the author(s) only and do not necessarily reflect those of the European Union or CINEA. Neither the European Union nor the granting authority can be held responsible for them. D.C. acknowledges the support of the Fonds de la Recherche Scientifique — FNRS [CR 40016260].

Appendix A. Parameters and uncertainties of the economic model

See Table A.1.

Appendix B. Cost values for each case

The comparison of HRES configurations, with the presentation of energy and cost values for each case, is presented in the three tables below. Tables B.1, B.2, B.3 show the results of the hospital, office and hotel respectively.

Table A.1
Uncertainty characterization of the parameters in the economic model. All the uncertainty distributions are uniform.

parameter	mean	std	unit	Ref.
Ambient conditions				
ambient temperature, T_{amb}	var[1]	0.4	°C	[33]
Energy costs				
hourly elec. price range	151 – 305	13.9 – 28	€/MWh	[66]
gas price	82	22.6	€/MWh	[40,66]
PV array				
$CAPEX_{PV}$	475	125	€/kW_p	[40]
$OPEX_{PV}$	17.5	1.5	€/kW_p/year	[40]
Battery				
$CAPEX_{bat}$	228	126.5	€/kWh	[40,72]
$OPEX_{bat}$	21.5	6.5	€/kWh/year	[40,72]
Heat pump				
$CAPEX_{HP}$	550	250	€/kW_{th}	[73]
$OPEX_{HP}$	0.6	0.6	€/kW_{th}/year	[73]
COP_{HP}	var[2]	0.25	—	[48]
DC/DC, DC/AC				
$CAPEX_{DC/DC}$	100	50	€/kW	[40]
$OPEX_{DC/DC}$, $OPEX_{DC/AC}$	3	2	%CAPEX	[40]
$\eta_{DC/DC}$	92.5	1.5	%	[74]
$CAPEX_{DC/AC}$	125	75	€/kW	[40]
$\eta_{DC/AC}$	90	0.5	%	[75]
Electrical steam generator				
$CAPEX_{ESG}$	450	150	€/kW_{th}	[38,76,77]
$OPEX_{ESG}$	16	1.6	€/kW_{th}/year	[38,76,77]
mGT				
$CAPEX_{mGT}$	1148	115	€/kW_e	[71,78]
$OPEX_{mGT}$	14	1.4	€/MWh	[53,71]
ICE				
$CAPEX_{ICE}$	683	68	€/kW_e	[71]
$OPEX_{ICE}$	26	2.6	€/MWh	[71]
Economic parameters				
interest rate, i	6	2	%	[40]
inflation rate, f	2	2	%	[79]

1 Ambient conditions vary every hour of the year.
2 COP is a function of T_{amb} and varies every hour of the year.

Table B.1
Comparison of HRES configurations for the hospital case. The HRES coupled with an mGT shows the lowest cost and highest SSR due to its ability to generate steam and run the heat pump and steam generator with its generated electrical power. The mHAT shows the same results as the mGT because it is used only 0.1% of the year.

parameters	without PM	ICE	mGT	mGT-wet	mHAT
Energy [MWh]					
Elec. by PV	2660	2660	2660	2660	2660
grid elec. for power	8140	8120	8120	8140	8120
grid elec. for heat	8940	3690	3290	4650	3290
Units cost [€/MWh]					
total and replacement	18	18.7	19.5	20.1	19.7
PV	8	8.1	8	8.1	8.1
PV DC/DC	1.4	1.4	1.4	1.4	1.4
battery	–	–	–	–	–
battery DC/DC	–	–	–	–	–
HP	2.2	1.7	1.6	1.8	1.6
PM	–	1.4	2.4	2.4	2.6
DC/AC	1.4	1.4	1.4	1.4	1.4
ESG	5	4.7	4.7	5.1	4.7
Grid, gas cost [€/MWh]					
grid cost for elec.	107.1	107.0	106.9	107.1	106.9
gas cost for PM	–	49.7	52.8	51.5	52.8
grid cost for HP	23.6	0.1	0.1	0.1	0.1
grid cost for heater	0.7	0.2	0.3	0.1	0.2
grid cost for steam	94.4	49.7	44.3	62.2	44.3
Objectives					
LCOX [€/MWh]	244	227.3	226.9	244.3	227.5
SSR [%]	28.1	28.3	28.3	28.2	28.3

Table B.2
Comparison of HRES configurations for the office case. The HRES with ICE presents the lowest LCOX followed by the mGT and case without PM. The mHAT shows the highest optimized cost and SSR as it increases grid independence but also gas cost.

parameters	without PM	ICE	mGT	mGT-wet	mHAT
Energy [MWh]					
Elec. by PV	1710	1650	1649	1642	1876
grid elec. for power	4000	3660	3695	3610	2552
grid elec. for heat	323	46.6	60.9	60.8	42.8
Units cost [€/MWh]					
total and replacement	20.7	22.7	24.5	25.4	27.7
PV	12.6	12.2	12.2	12.1	13.9
PV DC/DC	2.2	2.1	2.1	2.1	2.4
battery	–	–	–	0.01	–
battery DC/DC	–	–	–	–	–
HP	3.0	2.1	1.5	2.5	1.8
PM	–	3.5	5.9	5.9	6.4
DC/AC	2.9	2.8	2.8	2.8	3.2
ESG	–	–	–	–	–
Grid, gas cost [€/MWh]					
grid cost for elec.	124.7	112.7	113.9	110.9	79.5
gas cost for PM	–	17.9	16.2	20.4	58.1
grid cost for HP	9.1	1.1	1.5	1.5	0.9
grid cost for heater	2.4	0.5	0.6	0.5	0.6
grid cost for steam	–	–	–	–	–
Objectives					
LCOX [€/MWh]	156.9	154.9	156.6	158.8	170.5
SSR [%]	29.2	35.2	34.5	36.0	54.8

Table B.3
Comparison of HRES configurations for the hotel building.

parameters	without PM	ICE	mGT	mGT-wet	mHAT
Energy [MWh]					
Elec. by PV	1170	877	878	131	1029
grid elec. for power	1390	152	208	210.5	827
grid elec. for heat	943	17.5	51.7	39.2	455
Units cost [€/MWh]					
total and replacement	35	32.7	37.3	22.6	42.5
PV	18.6	13.95	13.97	2.1	16.4
PV DC/DC	3.24	2.43	2.43	0.36	2.85
battery	–	–	–	–	–1
battery DC/DC	–	–	–	–	–
HP	8.9	5.6	5.08	5.5	5.6
PM	–	7.5	12.6	12.6	13.9
DC/AC	4.23	3.22	3.22	2.	3.75
ESG	–	–	–	–	–
Grid, gas cost [€/MWh]					
grid cost for elec.	95.4	9.9	13.4	14	54.8
gas cost for PM	–	170.6	156.7	205.8	75.2
grid cost for HP	66.3	0.83	2.7	2.4	30.4
grid cost for heater	1.83	0.27	0.69	0.17	0.53
grid cost for steam	–	–	–	–	–
Objectives					
LCOX [€/MWh]	198.4	223.9	226.3	261.4	203.3
SSR [%]	40.4	93.5	91	91	64.5

Appendix C. Capacities of office and hotel cases

The capacities of the configurations in the office case are presented in Fig. C.1. All the designs show similar behavior. The PV and battery capacities increase as the LCOX and SSR rise. Moreover, at the maximum LCOX, the heat pump capacity is forced to zero for the case without PM to allow for the battery to store more electricity. The heat pump capacity for the cases that employ a PM at the maximum LCOX to enable the PM use more electricity to satisfy the demand and less to run the heat pump. However, the heat pump is kept almost constant for the majority of the designs. The ICE presents lower heat pump capacity than the case without PM at low LCOX. This sharp increase of the Pareto fronts at low LCOX (especially in the case without PM between 29.5% and 35% of SSR) is explained by the increase in PV capacity at the same region.

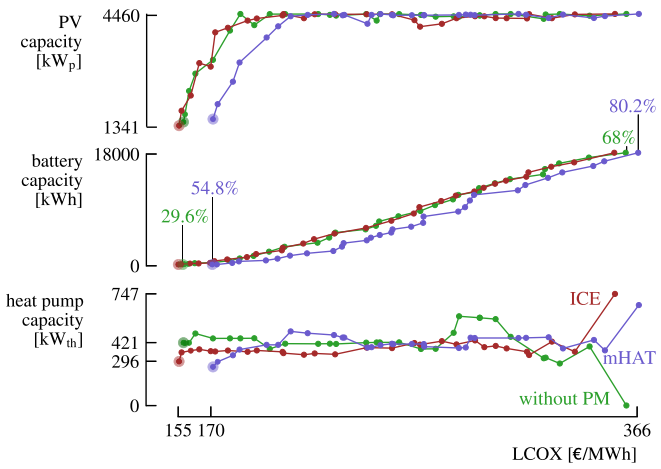

Fig. C.1. PV, battery and heat pump capacities as a function of LCOX for the case without PM, ICE and mHAT. In the selected design (see the circles), the PV capacity is maximized for all cases. The ICE shows lower heat pump capacity at low LCOX than the system without PM.

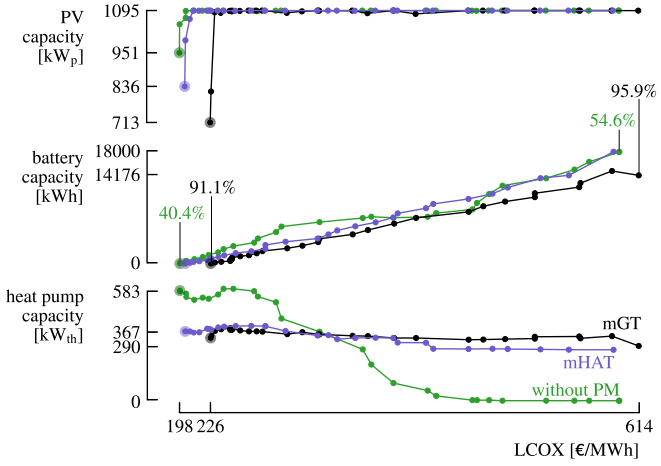

Fig. C.2. PV, battery and heat pump capacities as a function of the LCOX for the case without PM, mGT and mHAT. In the selected design (see the circles), the PV capacity is not maximum for all cases. The presence of PM lowers the optimal PV capacity to utilize more electricity which is produced by the heat-driven PM.

The capacities in the Pareto fronts for the mGT, mHAT and case without PM are presented in Fig. C.2. The other prime mover cases are not shown, as they present similar trends. As the LCOX and SSR increase, the PV and battery capacity rise to satisfy higher percentages of demanded electricity. The PV capacities reach the maximum PV capacity, which was set by the optimizer (see Table 2) at low LCOX. For the mGT case at optimum LCOX the PV is lower than the case without PM. As the PM is forced into the HRES design and its capacity is fixed, the optimizer decreases the PV capacity to lower the cost. This is a result of the EMS. The prime mover is heat driven, thus the produced electricity satisfies the demand and then is stored or lost. As the battery capacity is zero at the optimal point, with higher PV capacity, more electricity from PM is lost. As a result, the PV capacity is decreased and more electricity is produced, influenced by the gas price. The behavior of mHAT's PV capacity falls in the middle of the case without PM and the mGT highlighting that the wet mode of this configuration is not utilized sufficient times and the system presents a behavior in between the case without PM and the mGT. The mHAT system is analyzed thoroughly in the next paragraph. The battery capacity experiences a monotonous increase towards the maximum value and maximum SSR. The presence of prime mover decreases the required heat pump capacity. However, the heat pump capacity remains constant as the LCOX increases due to the fact that when a PM is employed, its operation is connected with the heat pump. More specifically, when the electricity demand is covered by the PV and the heat demand remains, the PM runs to produce heat and use its electricity output to run the heat pump.

Data availability

Data will be made available on request.

References

[1] International Energy Agency (IEA). Solar PV. 2025, Web page, URL: https://www.iea.org/energy-system/renewables/solar-pv. Accessed 3 December 2025.
[2] International Energy Agency Photovoltaic Power Systems Programme (IEA-PVPS). Trends in PV applications 2024. 2024, Web report, URL: https://iea-pvps.org/trends_reports/trends-in-pv-applications-2024/. Accessed 3 December 2025.
[3] International Energy Agency (IEA). Grid-scale storage. 2023, URL: https://www.iea.org/energy-system/electricity/grid-scale-storage.
[4] Uddin M, Mo H, Dong D, Elsawah S, Zhu J, Guerrero JM. Microgrids: A review, outstanding issues and future trends. Energy Strat Rev 2023;49:101127. http://dx.doi.org/10.1016/j.esr.2023.101127.
[5] Boruah D, Chandel SS. Techno-economic feasibility analysis of a commercial grid-connected photovoltaic plant with battery energy storage-achieving a net zero energy system. J Energy Storage 2024;77:109984. http://dx.doi.org/10.1016/j.est.2023.109984.
[6] Isa NM, Das HS, Tan CW, Yatim AHM, Lau KY. A techno-economic assessment of a combined heat and power photovoltaic/fuel cell/battery energy system in Malaysia hospital. Energy 2016;112:75–90. http://dx.doi.org/10.1016/j.energy.2016.06.056, URL: https://www.sciencedirect.com/science/article/pii/S0360544216308301.
[7] Lund H, Østergaard PA, Connolly D, Mathiesen BV. Smart energy and smart energy systems. Energy 2017;137:556–65. http://dx.doi.org/10.1016/j.energy.2017.05.123, URL: https://www.sciencedirect.com/science/article/pii/S0360544217308812.
[8] Taghavifar H, Zomorodian ZS. Techno-economic viability of on grid micro-hybrid PV/wind/Gen system for an educational building in Iran. Renew Sustain Energy Rev 2021;143(C). http://dx.doi.org/10.1016/j.rser.2021.110877, URL: https://ideas.repec.org/a/eee/rensus/v143y2021ics1364032121001714.html.
[9] Ji C. Design, techno-economic feasibility analysis, and sensitivity study of an off-grid hybrid microgrid for developing communities. Renew Energy 2025;239:121956. http://dx.doi.org/10.1016/j.renene.2024.121956, URL: https://www.sciencedirect.com/science/article/pii/S096014812402024X.
[10] Masrur H, Howlader HOR, Elsayed Lotfy M, Khan KR, Guerrero JM, Senjyu T. Analysis of techno-economic-environmental suitability of an isolated microgrid system located in a remote island of Bangladesh. Sustainability 2020;12(7). http://dx.doi.org/10.3390/su12072880, URL: https://www.mdpi.com/2071-1050/12/7/2880.
[11] Amini S, Bahramara S, Golpîra H, Francois B, Soares J. Techno-economic analysis of renewable-energy-based micro-grids considering incentive policies. Energies 2022;15(21). http://dx.doi.org/10.3390/en15218285, URL: https://www.mdpi.com/1996-1073/15/21/8285.
[12] Güven AF, Rizk-Allah RM. Optimal configuration framework of hybrid renewable energy technologies-based hydrogen energy storage system assessment using enhanced artificial rabbit algorithm. Energy 2025;326:135408. http://dx.doi.org/10.1016/j.energy.2025.135408.
[13] Güven AF, Özdal Mengi O, Bajaj M, Azar AT, El-Shafai W. Integrated techno-economic optimization and metaheuristic benchmarking of grid-connected hybrid renewable energy systems using real-world load and climate data. E-Prime - Adv Electr Eng Electron Energy 2025;13:101099. http://dx.doi.org/10.1016/j.prime.2025.101099.
[14] Güven AF, Abdelaziz AY, Samy MM, Barakat S. Optimizing energy dynamics: A comprehensive analysis of hybrid energy storage systems integrating battery banks and supercapacitors. Energy Convers Manage 2024. http://dx.doi.org/10.1016/j.enconman.2024.118560.
[15] Kushwaha PK, Bhattacharjee C. Integrated techno-economic-environmental design of off-grid microgrid model for rural power supply in India. J Inf Optim Sci 2022;43(1):37–54. http://dx.doi.org/10.1080/02522667.2022.2032557.
[16] Güven AF, Hassan MH, Kamel S. Optimization of a hybrid microgrid for a small hotel using renewable energy and EV charging with a quadratic interpolation beluga whale algorithm. Neural Comput Appl 2025;37:3973–4008. http://dx.doi.org/10.1007/s00521-024-10865-0.

[17] International Energy Agency (IEA). World Energy Outlook 2022. 2022, URL: https://www.iea.org/reports/world-energy-outlook-2022, Place: Paris.

[18] Salman CA, Naqvi M, Thorin E, Yan J. Gasification process integration with existing combined heat and power plants for polygeneration of dimethyl ether or methanol: A detailed profitability analysis. Appl Energy 2018;226:116–28. http://dx.doi.org/10.1016/j.apenergy.2018.05.069, URL: https://www.sciencedirect.com/science/article/pii/S0306261918307864.

[19] Sheykhi M, Chahartaghi M, Pirooz AAS, Flay RGJ. Investigation of the effects of operating parameters of an internal combustion engine on the performance and fuel consumption of a CCHP system. Energy 2020;211:119041. http://dx.doi.org/10.1016/j.energy.2020.119041, URL: https://www.sciencedirect.com/science/article/pii/S0360544220321484.

[20] Alexis GK, Liakos P. A case study of a cogeneration system for a hospital in Greece. Economic and environmental impacts. Appl Therm Eng 2013;54(2):488–96. http://dx.doi.org/10.1016/j.applthermaleng.2013.02.019, URL: https://www.sciencedirect.com/science/article/pii/S1359431113001245.

[21] De Paepe W, Montero Carrero M, Bram S, Parente A, Contino F. Toward higher micro gas turbine efficiency and flexibility—Humidified micro gas turbines: A review. ASME J Eng Gas Turbines Power 2018;140(8):081702. http://dx.doi.org/10.1115/1.4038365, Publisher: American Society of Mechanical Engineers (ASME).

[22] Kumar N, Karmakar S. Techno-economics of a trigeneration HRES; a step towards sustainable development. Renew Energy 2022;198:833–40. http://dx.doi.org/10.1016/j.renene.2022.08.107, URL: https://www.sciencedirect.com/science/article/pii/S0960148122012812.

[23] Ismail MS, Moghavvemi M, Mahlia TMI. Genetic algorithm based optimization on modeling and design of hybrid renewable energy systems. Energy Convers Manage 2014;85:120–30. http://dx.doi.org/10.1016/j.enconman.2014.05.064, URL: https://www.sciencedirect.com/science/article/pii/S0196890414004750.

[24] Comodi G, Renzi M, Cioccolanti L, Caresana F, Pelagalli L. Hybrid system with micro gas turbine and PV (photovoltaic) plant: Guidelines for sizing and management strategies. Energy 2015;89:226–35. http://dx.doi.org/10.1016/j.energy.2015.07.072, URL: https://www.sciencedirect.com/science/article/pii/S0360544215009676.

[25] Weerakoon AHS, Assadi M. Micro gas turbines in the global energy landscape: Bridging the techno-economic gap with comparative and adaptive insights from internal combustion engines and renewable energy sources. Energies 2024;17(21). http://dx.doi.org/10.3390/en17215457, URL: https://www.mdpi.com/1996-1073/17/21/5457.

[26] Ferrari ML, Gini L, Maccarini S. Laboratory tests in cyber-physical mode for an energy management system including renewable sources and industrial symbiosis. In: ASME turbo expo 2024: Turbomachinery technical conference and exposition. 2024, http://dx.doi.org/10.1115/GT2024-128015.

[27] Montero Carrero M, De Paepe W, Bram S, Musin F, Parente A, Contino F. Humidified micro gas turbines for domestic users: An economic and primary energy savings analysis. Energy 2016;117:429–38. http://dx.doi.org/10.1016/j.energy.2016.04.024, URL: https://www.sciencedirect.com/science/article/pii/S0360544216304303, The 28th International Conference on Efficiency, Cost, Optimization, Simulation and Environmental Impact of Energy Systems - ECOS 2015.

[28] Montero Carrero M, Sánchez I, De Paepe W, Parente A, Contino F. Is there a future for small-scale cogeneration in europe? Economic and policy analysis of the internal humid air turbine cycles. Energies 2019;12(3):1–27, Publisher: MDPI.

[29] Coppitters D, Contino F, El-Baz A, Breuhaus P, De Paepe W. Techno-economic feasibility study of a solar-powered distributed cogeneration system producing power and distillate water: Sensitivity and exergy analysis. Renew Energy 2020;150:1089–97. http://dx.doi.org/10.1016/j.renene.2019.10.105, URL: https://www.sciencedirect.com/science/article/pii/S0960148119316027.

[30] Coppitters D, Contino F. Optimizing upside variability and antifragility in renewable energy system design. Sci Rep 2023;13(1):9138, Publisher: Nature Publishing Group UK London.

[31] Contino F, Moret S, Limpens G, Jeanmart H. Whole-energy system models: The advisors for the energy transition. Prog Energy Combust Sci 2020;81:100872, Publisher: Elsevier.

[32] Mavromatidis G, Orehounig K, Carmeliet J. A review of uncertainty characterisation approaches for the optimal design of distributed energy systems. Renew Sustain Energy Rev 2018;88:258–77. http://dx.doi.org/10.1016/j.rser.2018.02.021, URL: https://www.sciencedirect.com/science/article/pii/S1364032118300510.

[33] Wilcox S, Marion W. Users manual for TMY3 data sets. 2008, Publisher: National Renewable Energy Laboratory Golden, CO.

[34] CodeMinders. Weather similarity. 2023, URL: https://www.codeminders.com/weather_similarity/#.

[35] National Renewable Energy Laboratory. Commercial and residential hourly load profiles for all TMY3 locations in the United States. 2014, http://dx.doi.org/10.25984/1788456.

[36] European Commission. Potential for heating and cooling efficiency in the Brussels-Capital Region. 2020, URL: https://energy.ec.europa.eu/system/files/2021-10/be-bru_ca_2020_en.pdf.

[37] Chiang C-Y, Yang R, Yang K-H, Lee S-K. Performance analysis of an integrated heat pump with air-conditioning system for the existing hospital building application. Sustainability 2017;9(4):530. http://dx.doi.org/10.3390/su9040530, URL: https://www.mdpi.com/2071-1050/9/4/530.

[38] FBL. 2020, URL: https://www.fulton.com/products/fbl/.

[39] Virtanen P, Gommers R, Oliphant TE, Haberland M, Reddy T, Cournapeau D, et al. SciPy 1.0: Fundamental algorithms for scientific computing in Python. Nature Methods 2020;17:261–72. http://dx.doi.org/10.1038/s41592-019-0686-2.

[40] Coppitters D, De Paepe W, Contino F. Robust design optimization of a photovoltaic-battery-heat pump system with thermal storage under aleatory and epistemic uncertainty. Energy 2021;229:120692. http://dx.doi.org/10.1016/j.energy.2021.120692, URL: https://www.sciencedirect.com/science/article/pii/S0360544221009403.

[41] Holmgren WF, Hansen CW, Mikofski MA. Pvlib python: A python package for modeling solar energy systems. J Open Source Softw 2018;3:884.

[42] De Soto W, Klein SA, Beckman WA. Improvement and validation of a model for photovoltaic array performance. Sol Energy 2006;80(1):78–88. http://dx.doi.org/10.1016/j.solener.2005.06.010.

[43] SolarHub - PV module details: SPR-X19-240-BLK - by SunPower. 2024, URL: https://solarhub.com/solarhub_products/53379-SPR-X19-240-BLK-SunPower.

[44] Expected lifespan of a solar inverter | RenewGenius. 2023, URL: https://renewgenius.com/components/expected-lifespan-of-a-solar-inverter/, Section: Components.

[45] How long do residential solar inverters last? Pv Mag Int 2024. URL: https://www.pv-magazine.com/2024/07/24/how-long-do-residential-solar-inverters-last-4/.

[46] Blaifi S, Moulahoum S, Colak I, Merrouche W. An enhanced dynamic model of battery using genetic algorithm suitable for photovoltaic applications. Appl Energy 2016;169:888–98, Publisher: Elsevier.

[47] Phurailatpam C, Rajpurohit BS, Wang L. Planning and optimization of autonomous DC microgrids for rural and urban applications in India. Renew Sustain Energy Rev 2018;82:194–204. http://dx.doi.org/10.1016/j.rser.2017.09.022, URL: https://www.sciencedirect.com/science/article/pii/S1364032117312509.

[48] Staffell I, et al. A review of domestic heat pumps. Energy & Environ Sci 2012;5(11):9291–306, Publisher: Royal Society of Chemistry.

[49] Gaitanis A, Tiwari RN, De Paepe W, Ferrari ML, Contino F, Breuhaus P. Operational strategies of two-spool micro gas turbine with alternative fuels: A performance assessment. J Eng Gas Turbines Power 2024;146(091011). http://dx.doi.org/10.1115/1.4064798.

[50] Lund H, Thorsen JE, Jensen SS, Madsen FP. Fourth-generation district heating and motivation tariffs. ASME Open J Eng 2022;1(011002). http://dx.doi.org/10.1115/1.4053420.

[51] Gaitanis A, Contino F, De Paepe W. Optimal waste heat recovery through humidification in 2-spool micro gas turbines: A comparative study of advanced humidified cycles. Energy 2025;332:136976. http://dx.doi.org/10.1016/j.energy.2025.136976, URL: https://www.sciencedirect.com/science/article/pii/S0360544225026180.

[52] Desideri U, Maria FD. Water recovery from hat cycle exhaust gas: A possible solution for reducing stack temperature problems. Int J Energy Res 1997;21:809–22.

[53] Tilocca G, Sánchez D, Torres-García M. Application of the theory of constraints to unveil the root causes of the limited market penetration of micro gas turbine systems. Energy 2023;278:127717. http://dx.doi.org/10.1016/j.energy.2023.127717, URL: https://linkinghub.elsevier.com/retrieve/pii/S0360544223011118.

[54] 2G energy - cogeneration and CHP cogeneration. 2023, URL: https://2-g.com/en.

[55] Montero Carrero M, De Paepe W, Parente A, Contino F. T100 mGT converted into mHAT for domestic applications: Economic analysis based on hourly demand. Appl Energy 2016;164:1019–27, Publisher: Elsevier.

[56] Rijal N. Autoclave sterilization: Principle, procedure, types, uses • Microbe online. 2019, URL: https://microbeonline.com/autoclave-principle-procedure-types-and-uses/,

[57] Guide to optimal steam generation | Knowledge center. 2024, URL: https://www.steris.com/healthcare/knowledge-center/sterile-processing/guide-to-optimal-steam-generation.

[58] Steam sterilization | Disinfection & sterilization guidelines | Guidelines library | Infection control | CDC. 2019, URL: https://www.cdc.gov/infectioncontrol/guidelines/disinfection/sterilization/steam.html.

[59] Dion M, Parker W. Steam sterilization principles. 2013.

[60] The use of steam generators in the medical industry. 2024, URL: https://www.thomasnet.com/knowledge/the-use-of-steam-generators-in-the-medical-industry/.

[61] Hampel CA, Braun RJ. Off-design modeling of a microturbine combined heat & power system. Appl Therm Eng 2022;202:117670. http://dx.doi.org/10.1016/j.applthermaleng.2021.117670, URL: https://www.sciencedirect.com/science/article/pii/S1359431121010954.

[62] Li Y, Zhang G, Bai Z, Song X, Wang L, Yang Y. Backpressure adjustable gas turbine combined cycle: A method to improve part-load efficiency. Energy Convers Manage 2018;174:739–54. http://dx.doi.org/10.1016/j.enconman.2018.07.077, URL: https://linkinghub.elsevier.com/retrieve/pii/S0196890418308124.

[63] Coppitters D, Tsirikoglou P, De Paepe W, Kyprianidis K, Kalfas A, Contino F. RHEIA: Robust design optimization of renewable Hydrogen and dErIved energy cArrier systems. J Open Source Softw 2022;7(75):4370.

[64] Zakeri B, Syri S. Electrical energy storage systems: A comparative life cycle cost analysis. Renew Sustain Energy Rev 2015;42:569–96. http://dx.doi.org/10.1016/j.rser.2014.10.011, URL: https://linkinghub.elsevier.com/retrieve/pii/S1364032114008284.

[65] Di Somma M, Yan B, Bianco N, Graditi G, Luh P, Mongibello L, et al. Multi-objective design optimization of distributed energy systems through cost and exergy assessments. Appl Energy 2017;204:1299–316. http://dx.doi.org/10.1016/j.apenergy.2017.03.105, URL: https://linkinghub.elsevier.com/retrieve/pii/S0306261917303483.

[66] Electricity prices in Belgium. 2023, URL: https://www.globalpetrolprices.com/Belgium/electricity_prices/.

[67] Ghaleb B, Asif M. Application of solar PV in commercial buildings: Utilizability of rooftops. Energy Build 2022;257:111774. http://dx.doi.org/10.1016/j.enbuild.2021.111774, URL: https://www.sciencedirect.com/science/article/pii/S0378778821010586.

[68] Dias V, Pochet M, Contino F, Jeanmart H. Energy and economic costs of chemical storage. Front Mech Eng 2020;6. URL: https://www.frontiersin.org/articles/10.3389/fmech.2020.00021.

[69] Grahn M, Malmgren E, Korberg AD, Taljegard M, Anderson JE, Brynolf S, et al. Review of electrofuel feasibility—cost and environmental impact. Prog Energy 2022;4(3):032010. http://dx.doi.org/10.1088/2516-1083/ac7937, Publisher: IOP Publishing.

[70] Coppitters D, De Paepe W, Contino F. Robust design optimization and stochastic performance analysis of a grid-connected photovoltaic system with battery storage and hydrogen storage. Energy 2020;213:118798. http://dx.doi.org/10.1016/j.energy.2020.118798, URL: https://www.sciencedirect.com/science/article/pii/S0360544220319058.

[71] Tilocca G, Sánchez D, Torres-García M, Escamilla-Perejón A, Minett S. A methodology to quantify product competitiveness and innovation requirements for micro gas turbine systems in hydrogen backup applications. In: Proceedings of the ASME turbo expo 2023: Turbomachinery technical conference and exposition. Cycle innovations, Vol. 5, Boston, Massachusetts, USA: ASME; 2023, http://dx.doi.org/10.1115/GT2023-102606, Issue: V005T06A017.

[72] Kebede AA, Coosemans T, Messagie M, Jemal T, Behabtu HA, Mierlo JV, et al. Techno-economic analysis of lithium-ion and lead-acid batteries in stationary energy storage application. J Energy Storage 2021;40:102748. http://dx.doi.org/10.1016/j.est.2021.102748, URL: https://www.sciencedirect.com/science/article/pii/S2352152X21004783.

[73] Hofmeister M, Guddat M. Techno-economic projections until 2050 for smaller heating and cooling technologies in the residential and tertiary sector in the EU. Luxembourg: Publications Office of the European Union; 2017, http://dx.doi.org/10.2760/110433.

[74] Taghvaee MH, Radzi MAM, Moosavain SM, Hizam H, Marhaban MH. A current and future study on non-isolated DC–DC converters for photovoltaic applications. Renew Sustain Energy Rev 2013;17:216–27. http://dx.doi.org/10.1016/j.rser.2012.09.023, URL: https://www.sciencedirect.com/science/article/pii/S1364032112005242.

[75] Rampinelli GA, Krenzinger A, Romero FC. Mathematical models for efficiency of inverters used in grid connected photovoltaic systems. Renew Sustain Energy Rev 2014;34:578–87. http://dx.doi.org/10.1016/j.rser.2014.03.047, URL: https://www.sciencedirect.com/science/article/pii/S1364032114002081.

[76] CES, CHPES, & CSSB modular steam generators | Chromalox. 2024, URL: https://www.chromalox.com/en/products-and-technologies/industrial-heaters-and-systems/steam-generators/steam-generators/modular-steam-generators.

[77] Electric and automatic steam generators | Ghidini. 2024, URL: https://www.ghidinisteam.com/products/1/products/electric-automatic-steam-generator.

[78] Malkamäki M, Jaatinen-Värri A, Honkatukia A, Backman J, Larjola J. A high efficiency microturbine concept. In: 11th European conference on turbomachinery fluid dynamics & thermodynamics ETC11, Madrid, Spain. 2015.

[79] Belgium inflation rate. 2023, URL: https://ycharts.com/indicators/belgium_inflation_rate.